UDC 533.6.013 :
629.735.014.16

TECHNICAL REPORT OF NATIONAL AEROSPACE LABORATORY

TR-197T

Wind Tunnel Investigations of the STOL Airplane, with Attention to the Relations between the Aerodynamic Characteristics and the Wake Structure

Norio INUMARU, Kiyomi KITAMURA, Nagakatsu KAWAHATA,
Hitoshi TAKAHASHI and Tomoaki SUZUKI

May. 1970

NATIONAL AEROSPACE LABORATORY

CHŌFU, TOKYO, JAPAN

List of NAL Technical Reports

TR-171T Simple Flow Characteristics Across a Strong Shock Wave	Kenneth K. YOSHIKAWA	Feb. 1969
TR-172 Measurements of Dynamic Stability Derivatives of Cones and Delta-Wings at High Speed	Mitsunori YANAGIZAWA	Feb. 1969
TR-173T The Coupling Effect of Radiative Heat on Convective Heat Transfer	Kenneth K. YOSHIKAWA	Feb. 1969
TR-174 Difference Method for Navier-Stokes Equation	Hajime MIYOSHI	Apr. 1969
TR-175 Stalling Characteristics of the NACA 0012 Aerofoil Section at Low Reynolds Numbers	Yasuharu NAKAMURA, Koji ISOGAI & Hiroshi EJIRI	Jun. 1969
TR-176 On the Vibration of Axial-flow Turbomachine Blades (I) Natural Frequency, Mode and Vibratory Stress Distribution	Toshio MIYACHI, Shoji HOSHIYA, Yasuyuki SOFUE, Saburo AMIHOSHI, Tadasuke IWABU & Katsumi TAKEDA	Jul. 1969
TR-177 Thrust Magnitude Control of Solid Rocket Motors —Characteristics Analysis and Small Motor Tests—	Tomifumi GODAI, Yoshinori YUZAWA, Katsuya ITO & Hisao NISHIMURA	Jul. 1969
TR-178 Necessary Conditions for the Optimal Weighting Matrices of Quadratic Performance Index to Maximize the Measure of the Controllable Set	Nagakatsu KAWAHATA	Jul. 1969
TR-179 Measurements of Transient Ablation of Teflon	Shigeaki NOMURA	Aug. 1969
TR-180 Measurement and Analysis of Atmospheric Turbulence over the SUZUKA Mountain Range	Kazuyuki TAKEUCHI, Koichi ONO, Kosaburo YAMANE, Toichi OKA & Tokuo SOTOZAKI	Aug. 1969
TR-181 Unsteady Surface Pressure on an Oscillating Aerofoil at High Mean Angles of Attack with Special Reference to Stall Flutter	Yasuharu NAKAMURA, Koji ISOGAI, & Hiroshi EJIRI	Aug. 1969
TR-182 On the Natural Viblation of Plates Restrained at Several Points	Taketoshi HANAWA, Yasuo TADA, Hideo IZUMI & Shinichi KOSHIDE	Sep. 1969
TR-183 Experimental Investigation of Strength of Axial Flow Compressor Blade Root —Pin Joints Lug having Clearance between Pin and Pin Hole—	Tameji IKEDA & Takashi YAMAGISHI	Sep. 1969
TR-184-T An Inproved Method of Designing and Calculating the Minimal Wave Drag Configuration by Supersonic and Moment-of-Area Rules	Kenneth K. Yoshikawa	Oct. 1969
TR-185 Thermal Characteristics of FPR Rocket Nosecone	Koichi OGAWA, Shinji ENDO	Nov. 1969
TR-186 The Analysis on Transmission-Line Rocket Antennas	Johji TABATA, Yoshio SAKURAI, Masao MIURA, Yoshitsugu MATSUZAKI & Norio TSUKAMOTO	Dec. 1969
TR-187 A Magnetic Attitude Measuring Instrument Applying the Holl Effect	Shigeru KIMURA, Johji TABATA & Yoshitsugu MATSUZAKI	Dec. 1969
TR-188 Analysis of Anisoelastic Errors of a Floated Single Degree of-Freedom Integrating	Masao OTSUKI, Hirokimi SHINGU, Johji TABATA, Takao SUZUKI & Shigeharu ENKYO	Jan. 1970

Wind Tunnel Investigations of the STOL Airplane, with Attention to the Relations Between the Aerodynamic Characteristics and the Wake Structure*

By

Norio INUMARU**, *Kiyomi KITAMURA**, Nagakatsu KAWAHATA**,
Hitoshi TAKAHASHI** and Tomoaki SUZUKI**

SUMMARY

Wind tunnel measurements have been carried out extensively on the flow field behind a powered model of the twin-propeller deflected slipstream STOL airplane.

By the use of new equipments in the measurement, spacial distributions of the flow velocity, down wash angle and side wash angle were obtained. Consequently the extraordinary deformation of the slipstream boundaries, and also the complicated movements of wake vortex systems have been recognized in the flow field. Furthermore by changing the direction of the propeller rotation, marked influences of the rotating flow on the flow field have been exhibited.

These observed experimental facts seem to have some connection with the nolinear aerodynamic characteristics of such a type of STOL airplane. The aerodynamic forces and moments of the model have also been obtained by the use of a sting type balance. Then, the probable relations among the relevant facts are discussed.

1. INTRODUCTION

It is well known that there are many types of configurations for the STOL airplane. Among these types we had chosen the twin-propeller deflected slipstream configurations as the subject of our study. Then, wind tunnel tests of this type of STOL airplane had been carried out successively. The results of these tests were presented in our previous reports.[1),2)] In view of our results, we supposed that for the practical use of this type of airplane several difficulties might exist in its characteristics. Some of those difficulties, namely the nonlinearities of several stability derivatives, could not be removed even though we had adopted counter rotation of the twin propellers. Of course, the power-off model did not exhibit those nonlinearities. It was supposed that those difficulties should be attributed to the effects of the slipstream.

In this work we have intended first to clarify the spacial developments of the wake flow field to the extent of the region from right behind the wing to the tailplane position. Secondly we have also intended to reconfirm the nonlinearities. Then, we have given our attention to the relations between those nonlinearities and alterations of the wake field.

2. MODEL AND WIND TUNELL

The airplane model used in this investigation was the same one used in the previous work, having a high wing and a conventional tailplane. The whole span of the wing was equipped with leading edge slats and double slotted flaps, and was covered with the propeller slipstream. A description of this model is presented in Table 1. A schematic drawing of the model showing three views is presented as fig. 1. The measurements were conducted with a tail-less model configuration for the sake of convenience in traversing the measuring sensor.

The wind tunnel used was the NAL large scale low speed tunnel which had the closed test section of 5.5 m width and 6.5 m height. In the test section, the location of the model was the same as in the previous investiga-

* Peceived Decmber 24, 1969
** V/STO Division

tions[1),2)].

Table 1. Description of model

Wing span	1.965 m
Total length	2.508 m
Height	0.3376 m
Max. Width of fuselage	0.300 m
Wing area	0.774 m^2
Aspect ratio	5.0
Taper ratio	0.6
Dihedral angle	2.0 Degrees
Wash-out	3.0 Degrees
Mean aerodynamic chord	0.402 m
Airfoil section	Mod. Root, 17% C, Tip 13% C
Wing incidence angle (Root)	4.0 Degrees
Leading edge slat	Whole span 15%, 25 Degrees
Flap Inner flap	Double slotted flap
Outer flap	Double slotted flap
Position of C.G.	M.A.C. 25%
Propeller Diameter	0.60 m
Number of blade	3
Description of propeller	NASA TN D-318, No. 1
Engine(Electric motor)	10 Ps×2

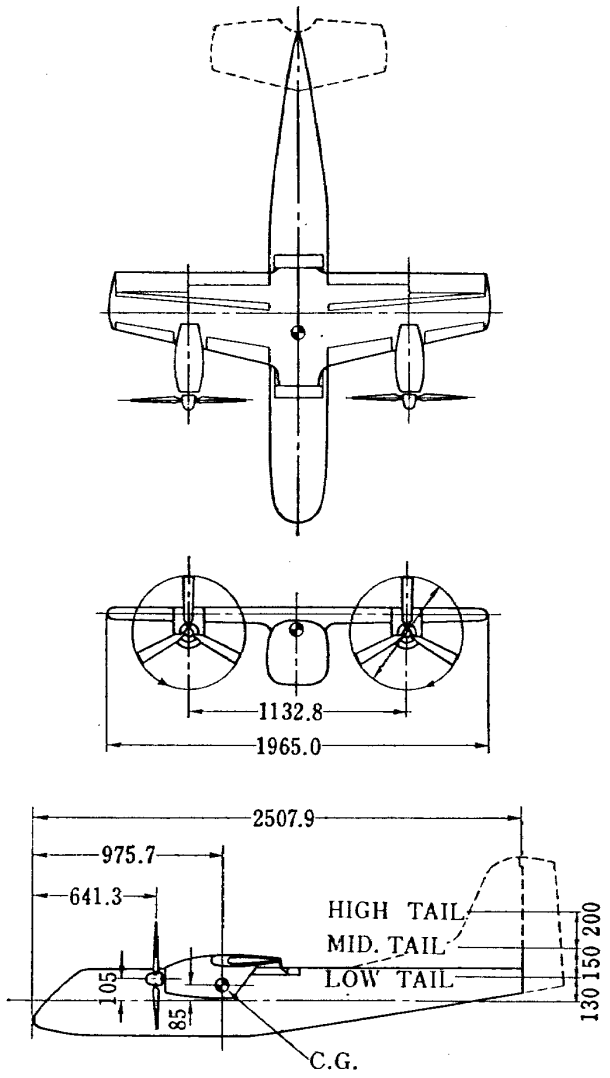

Fig. 1. Three views of the model

3. MEASURING SYSTEMS AND DATA REDUCTION

An outline of the measuring systems and the methods of processing the data are as follows;

(1) Velocitymeter with the Automatically Tracking Sensor

This velocitymeter was a new type of measuring system designed for surveying the spacial distribution of three flow parameters; flow velocity, down wash angle and side wash angle. The tracking sensor (a pyramid type pitot tube) can move in any direction around its pointed pitot head. In its working condition the pitot tube points continuously and automatically to the flow direction. This working condition is realized in cooperation with the whole systems including the amplifiers, servo motors, transducers etc...

In this way the pitot tube detects the dynamic pressure of the flow. Also the direction of the pitot tube indicates the flow direction at the point of its head. Then, the flow parameters are finally obtained as electrical output signals. For more detailed explanation of this velocitymeter, the reader is referred to the separate report[3)] written by the developer.

The idea of this velocitymeter was presented by Dr. Kobashi, Professor of Hokkaido University, who had developed this instrument with collaboration of Mr. Kawahata (one of the authors) and others.

(2) Traversing Apparatus

To survey the wake field we needed an apparatus for traversing the velocitymeter in the flow field. A longitudinally (in x direction) traversing system was designed and produced for this investigation. The laterally (in y, z direction) traversing systems were available

in the accessory of the wind tunnel. The traversing systems were available in the accessory of the wind tunnel. The traversing systems were joined together so that only one person working outside of the test section was able to control the measuring position. The coordinates of the measuring positions were detected and transformed into electrical signals by the use of potentiometers.

(3) Recording and Processing of the Data

The traversing survey was carried out along several planes (the vertical cross sections of the wake field) which were perpendicular to the free stream direction. On traversing the senser, we took the way of continuous traversing in y direction (along the horizontal line). Then we had put the electrical signals into a pen-writing oscillograph.

Afterwards, the continuously recorded data were translated manually into the physical quantities. Finally, the distributions of the flow parameters in the measured planes were put into the form of contour maps.

(4) Systems for the Supplementary Measurements

The nonlinear aerodynamic characteristics of the model were pointed out in our previous works.[1),2)] To confirm those nonlinearities again, the measurements of the six components of aerodynamic forces and moments of the tail-less model were also conducted. For these measurements the "six components sting balance" had been installed in the model fuselage. The model had been set up through the balance on the single strut which stood vertically in the tunnel test section. The aerodynamic coefficients were obtained through the AD converter and finally through the digital computer.

Measurements of flow turbulence were also conducted for the confirmation of the turbulence level in the two regions; inside and outside of the slipstream. The constant temperature hot wire anemometer was used and traversed together with the velocitymeter senser.

4. COEFFICIENTS AND SYMBOLS

X, Y, Z	cartesian coordinates
α	angle of attack
β	angle of side slip
C_L, C_D, C_Y	lift, drag, and side force coefficient
C_l, C_m, C_n	rolling, pitching and yawing moment coefficient
δ_f	angle of flap deflection (A/B: A and B indicate the deflection angle of inner flap and outer flap, respectively.)
V	flow velocity
q	free stream dynamic pressure
ε	down wash angle
σ	side wash angle
S	wing area
T	propeller thrust (per one engine)
T_c	$=T/qS$

5. CONTENTS OF THE MEASURMENTS

(1) Selection of the Measuring Conditions

The free stream velocity was settled at 18 m/sec, with the exceptions of propeller-off conditions. The Reynolds number was about 5×10^5 based on the wing aerodynamic chord. In the cases of propeller-off conditions the free stream velocity of 20 m/sec was adopted.

The rotational speed of the propellers were 4,500 rpm, and the pitch angle of each blade was 20 degrees, throughout the investigation. Then, the value of T_c was about 1.0 in the cases of the powered tests. Usually the directions of the propeller rotation were symmetrical as shown in Fig. 1. Additional tests were conducted with reversed rotation on the left propeller, to make sure of the rotational flow effects.

On the deflection of the flaps, the two cases

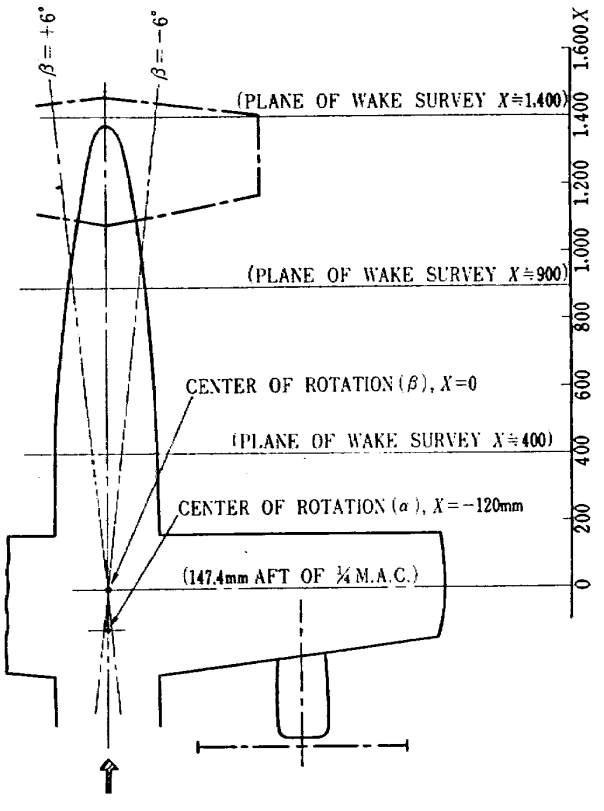

Fig. 2. Position of the model (X Coordinate)

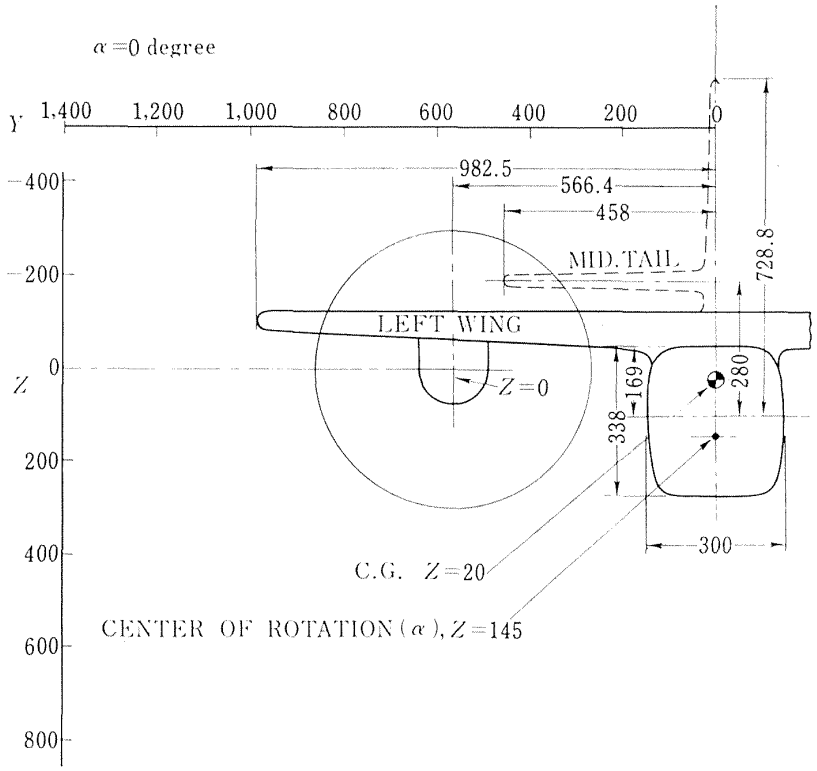

Fig. 3. Position of the model (Y, Z, Coordinate)

(0 degree and 60/20 degrees) were selected for the measurements.

In the wake survey the attitude of the model was held to be 0 or 8 degrees in α, and 0 or ± 6 degrees in β.

(2) Planes Selected for the Wake Survey, and Data Representations

The cartesian coordinates X, Y, Z had been set in space. The relative positions of the model in the space are given in Fig. 2 and in Fig. 3 (at $\alpha=0$ degree). In these figures the centers of rotation of the model in taking α and β are also given. Then, we took three vertical planes (Y-Z planes) fixed in the space, in which the wake survey was conducted. The X coordinates of those planes were about 400, 900 and 1,400 (in mm) respectively.

The distribution of three flow parameters V, ε and σ were presented in the form of contour maps. In other words, each selected condition had three vertical planes, and in each plane the three kinds of contour maps in V, ε and δ were obtained.

(3) List of Selected Conditions in the Wake Survey

The list of measurement conditions selected for this investigation is given in the last part of this report. (APPENDIX)

(4) Force Tests and Turbulence Measurements

As already explained in section 3. (4), the

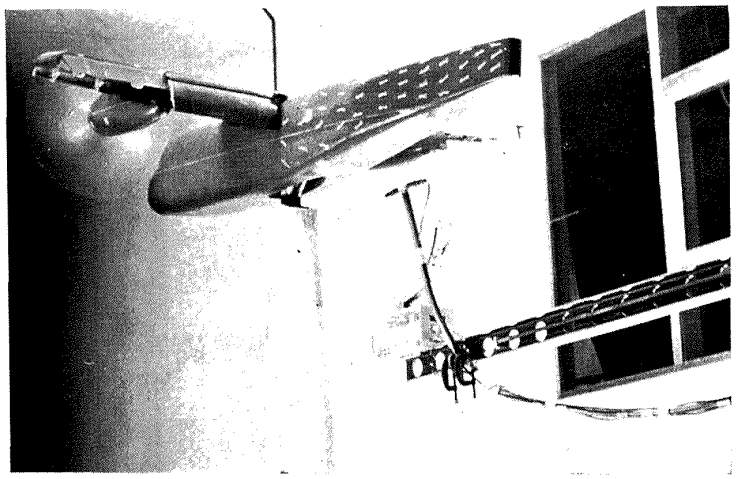

Fig. 4. Upstream view of the model and the senser

force tests were conducted in order to confirm the aerodynamic characteristics of the model. As usual, the variations of six aerodynamic coefficients were obtained with sweeping of α and β. The main parts of the results are presented and discussed in the section 9 of this report.

Supplemental measurements were carried out for the examination of the turbulence level in the wake field. A hot wire probe was put on the head of the traversing apparatus, apart a little from the senser of the velocitymeter. Then, it was traversed together with the velocitymeter senser, throughout the wake survey. The results are presented in a later section.

The upstream view of the apparatus is presented as Fig. 4.

6. DEFORMATION AND ROTATION OF THE SLIPSTREAM BOUNDARY

In this report, one of our aims is to confirm the deformation and development of the slipstream. There are many papers concerning the effects of the slipstream on the wing characteristics. In the theoretical work, the deformation of the slipstream boundary is customarily neglected.[4] Therefore, the deformation cannot be predicted. In the experimental work, there are few papers which have investigated the flow field around the wing or behind the wing. Also there are many papers concerning the rolling up of the wake sheet. But there are few papers which include the slipstream. So that, we have little information on this matter. Although our model has a specific type, the trends of our results may exist at least latently in the general cases.

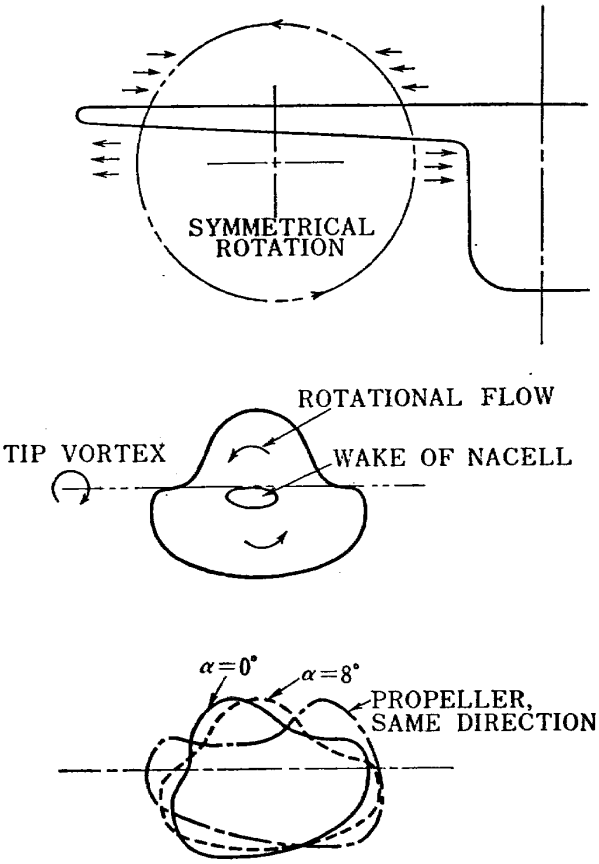

Fig. 5. The deformation and rotation of the slipstream cross section. ($\delta_f=0$, Left wing)

(1) In the Case of Clean Configuration

The total pressure of the flow in the slip-

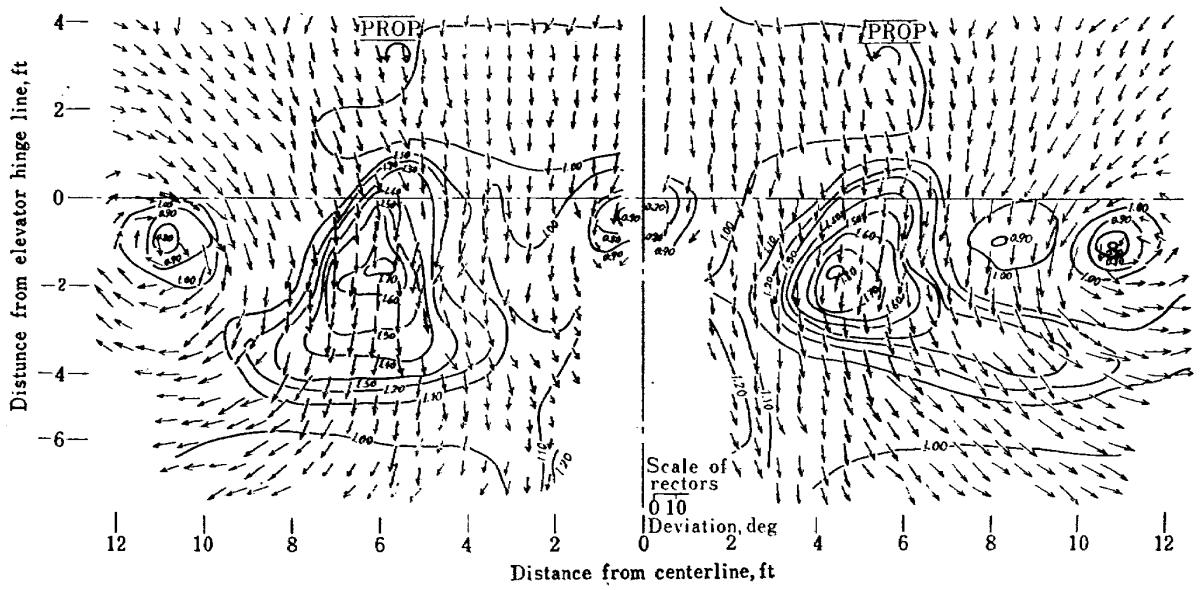

Fig. 6. Deformation of the slipstream boundary (Sweberg[6]) $\alpha=6.9$ deg $\delta_f=50$ deg. $T_c=0.06$ *At the tail plane position*

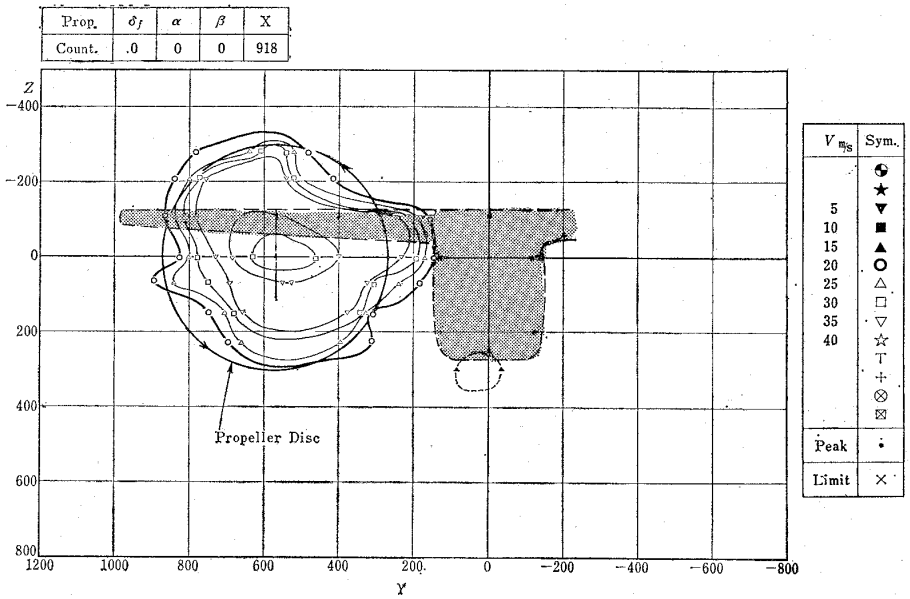

Fig. 7. Deformation of the slipstream boundary (sym. rotation)

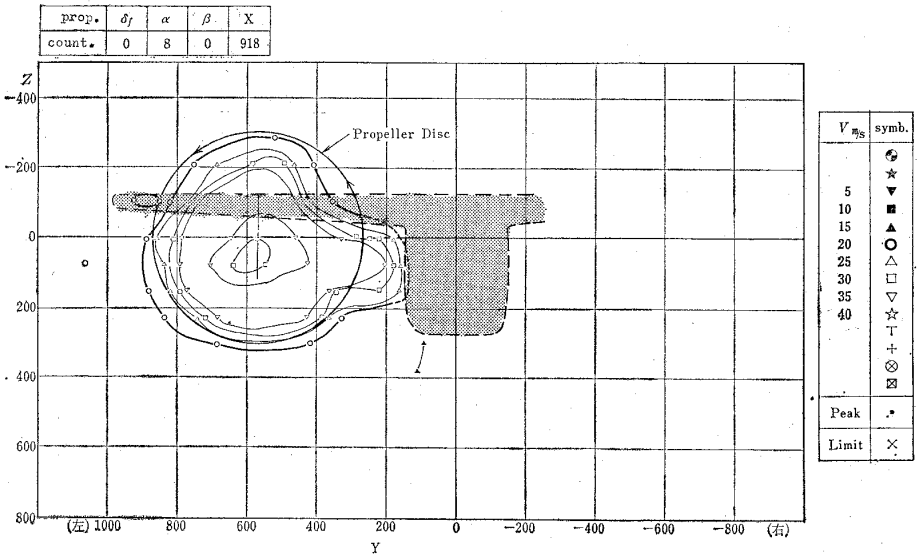

Fig. 8. Deformation of the slipstream boundary (sym. rotation)

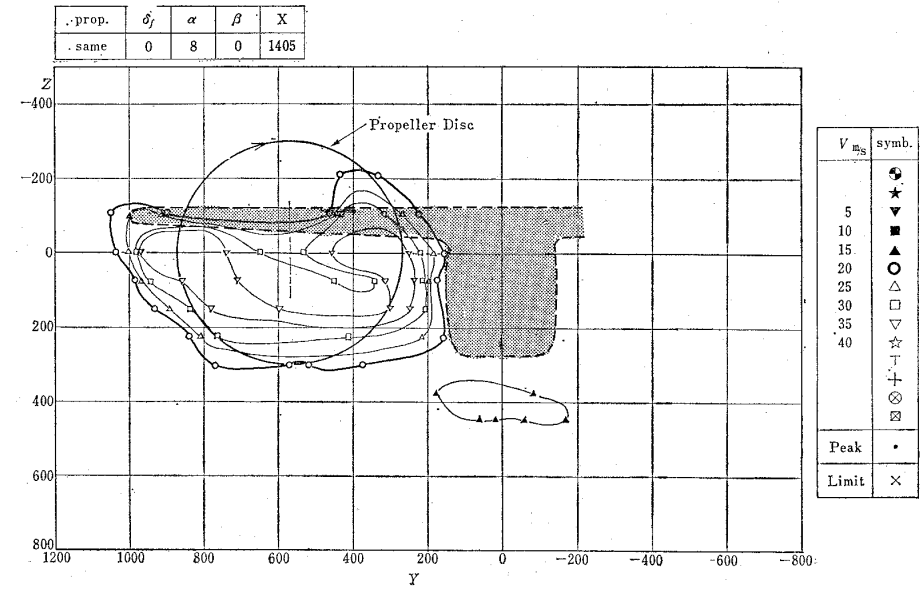

Fig. 9. Deformation of the slipstream boundary (same rot. direction)

stream is higher than in the free stream. The slipstream boundary separates the flow field into two regions. Through the boundary the velocity is discontinuous, but the pressure must be continuous. If the wing penetrates this boundary, a pressure difference between the two regions must arise, because of the alteration of the velocity field. Therefore, the boundary must deform around the wing anyway. Then, behind the wing the deformation may be observed in the wake survey. In view of our results, the deformation and rotation are considered to be of the form shown schematically in Fig. 5.

The wing cuts the slipstream cross section into two parts. The upper part becomes narrower, and the lower part becomes broader. These trends were early supposed by V. J. Stuper[5], and also expected by the author. The same experimental facts are also found in the paper of H. H. Sweberg[6] (see Fig. 6). Further more, the theoretical prediction of the deformation have recently presented in ref. 7.

The degree of the deformation and of the rotation are considerably altered by changing the angle of attack and the direction of the propeller rotation. At the small angles of attack, the rotation of the boundary cross section is in the same directions as the propeller, probably because of the rotational flow in the slipstream. Increasing the angles of attack acts to rotate conversely, probably because of

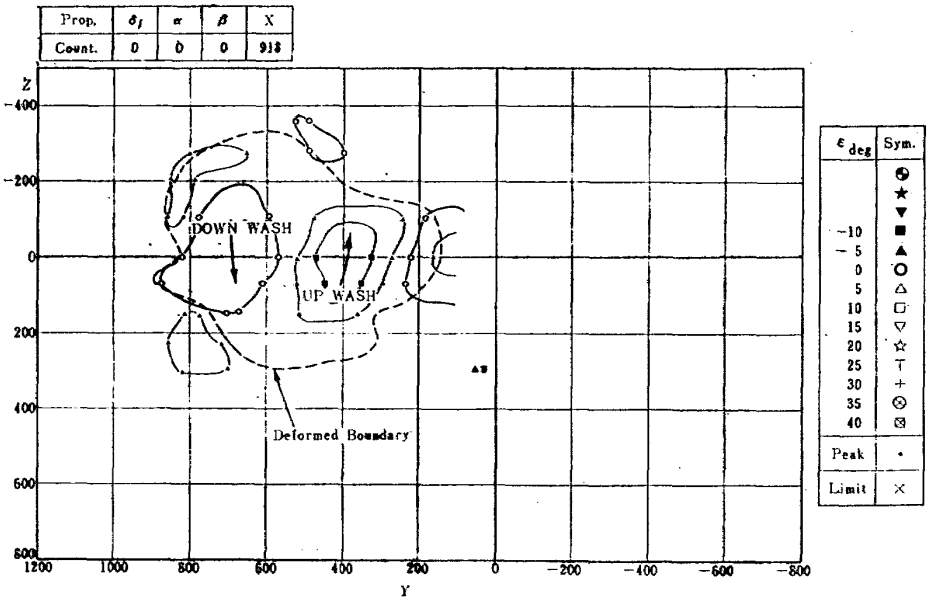

Fig. 10(a) Down wash field (in the case of Fig. 7)

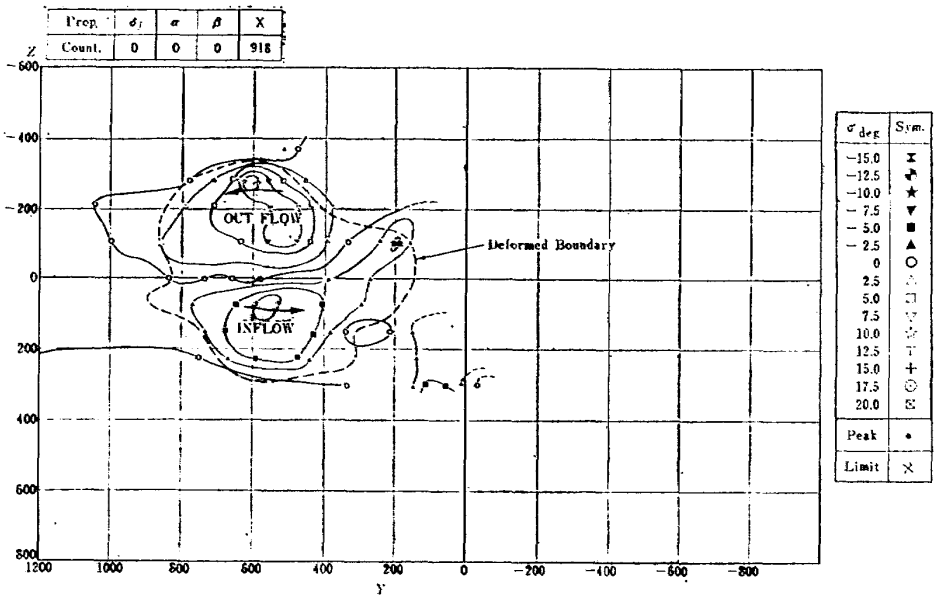

Fig. 10(b) Side wash field (in the case of Fig. 7)

the effects of the vortex sheet including the tip vortex. If we change the direction of the propeller rotation, the rotation is the same direction with the tip vortex in the left half of the wake field. Then, severe deformation and rotation of the boundary cross section are observed (see Fig. 5). The corresponding results of measurements are given in Figs. 7, 8, 9, for examples.

By the way, the mutual interference must be considered between the slipstream and the free stream in the wake field. In the present cases ($\delta_f=0$) the deformation and rotation are still smaller than the other cases (the cases of flaps deflected). In the slipstream, the circulating flow is verified in the distribution of ε and δ. For example, the contour maps of ε and σ in the case of Fig. 7 are given in Fig. 10 (a), (b). Although the representation of the contour maps is not intuitive, the circulating flow due to the propeller rotation is obvious. Furthermore, the gradient of σ at the top side of the boundary cross section is small in both sides. The gradient of ε at the upper and lower extremes is also small. Then we can also conclude that the slipstream is flowing just like a solid mass in almost the same direction as the outer flow, and the mutual interference may be not so apparent in this case.

(2) In the Cases of Flap Deflection ($\delta_f=60/20$ degrees)

In these cases, the inner flaps (double slotted flaps) are greater than the outer flaps (also they are the double slotted flaps) in their chord length and deflection angles, and have a higher lift force. Fig. 11 shows the schematic drawing of the flow field and developments of the slipstream boundary cross sections. At the inner part of the slipstream the strong down wash field is observed. Then, from the lower side of this part, the inflow arises toward the plane of symmetry (Fig. 11 (a)). By this inflow the lower part of the boundary seems to be extended toward the plane of symmetry. In this way, under the model fuselage, the extended edges of the boundary combine with each other and form a sheet of high speed flow (Fig. 11(b)). At the forward station of the wake field, nearly symmetrical flow field is observed around the plane of symmetry. However, in the region of further downstream this symmetry fades away successively, and complexities of the flow field arise.

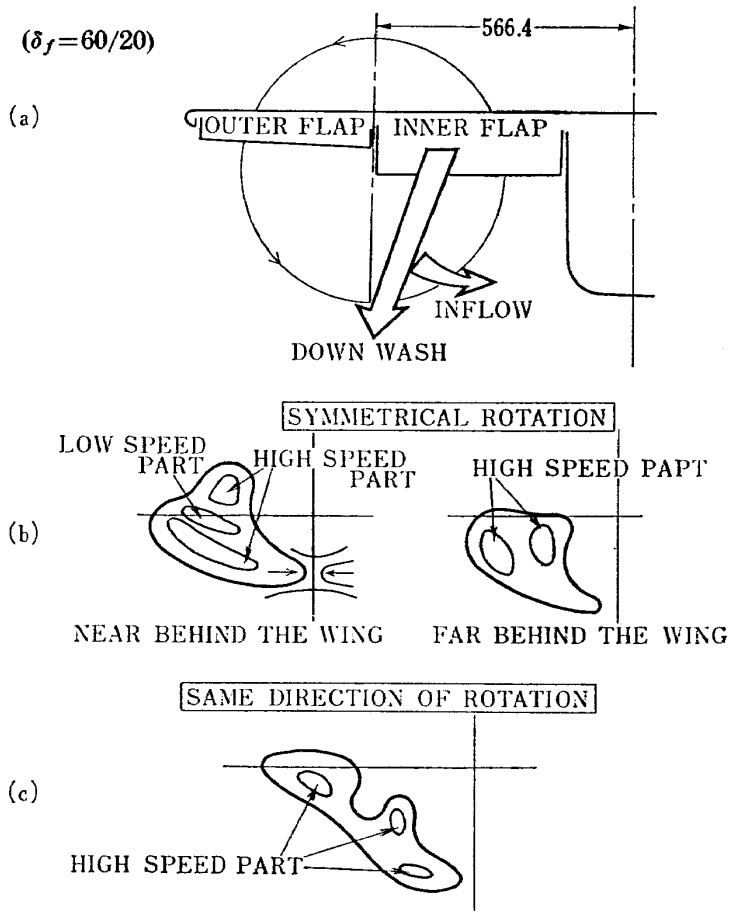

Fig. 11. The deformation and rotation of the slipstream cross section

In the cases of flapped configuration, the high speed regions which have been cut off by the wing into two parts, do not coalesce again into a single high speed region. There remains a low speed flat region between the two high speed region instead, in the initial phase of the wake development. This low speed region must be a flattened wake of the nacelle. The deformation and rotation of the boundary cross section is markedly severe. According to the successive development of the wake, the separated two high speed cores rotate clockwise to each other as shown in the sketch of Fig. 11(b). If we change the rotation direction of the propeller of the left wing, the deformation and rotation become more severe. In this case the high speed core which has passed below the wing, is more extended and sometimes may be split into two parts as indicated in Fig. 11(c). The experimental data corresponding to the above discussion are given in Figs. 12, 13, 14, 15. In Fig. 12(a) we see a strong down wash field due to the inner flaps. In Fig. 12(b) we can also point out the inflow region sketched in Fig. 11(a). Fig. 13(a), (b),(c) show us a successive development of high speed region in the case of symmetrical propeller rotation, corresponding to the sketch of Fig. 11(b). In the same way, Fig. 14(a), (b),(c) show us the results of measurements in the case of same rotational direction of propellers. The marked deformation and rotation of the slipstream can be seen. On the other hand, in the right hand side of Fig. 14(c), the similar velocity distribution as Fig. 13(c) can be seen. Therefore, it is likely that the change of the rotational direction of propeller does not affect much influences beyond the plane of symmetry. Fig. 15 is one of the similar data corresponding to the sketch of Fig. 11(c).

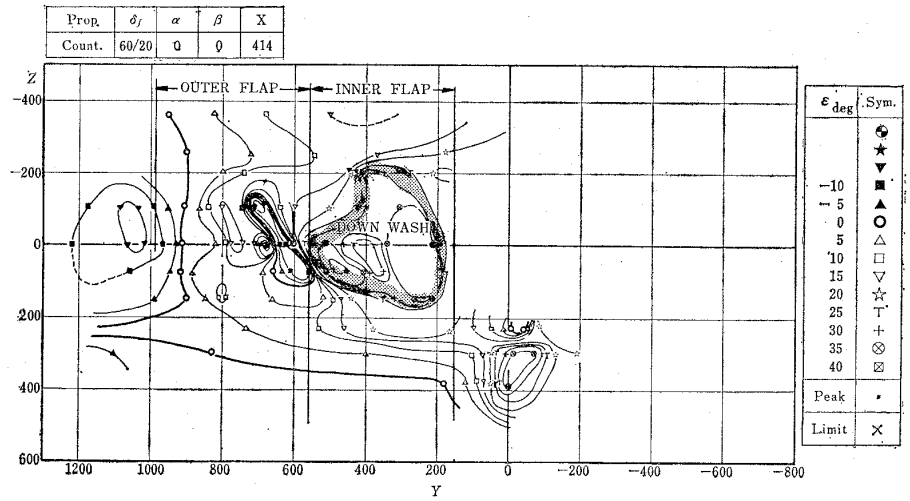

Fig. 12(a) Down wash field due to the inner flap (sym. rotation)

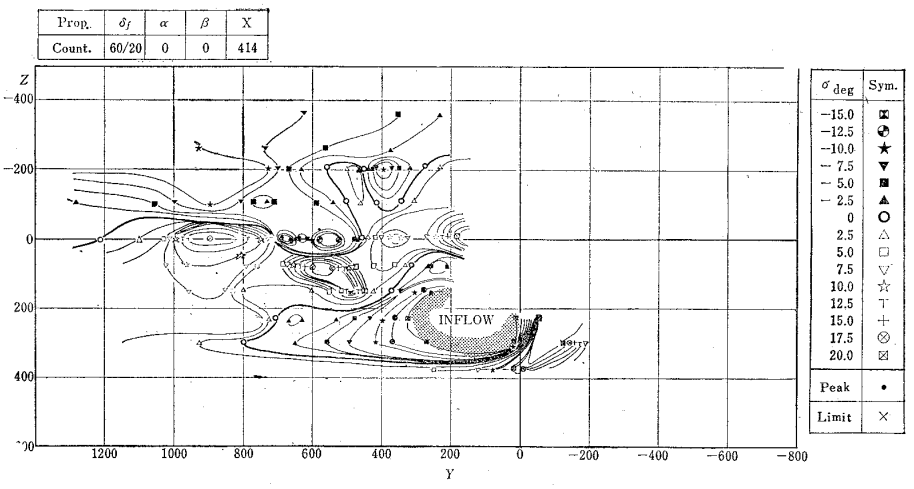

Fig. 12(b) Inflow region corresponding to Fig. 11(a) (sym. rotation)

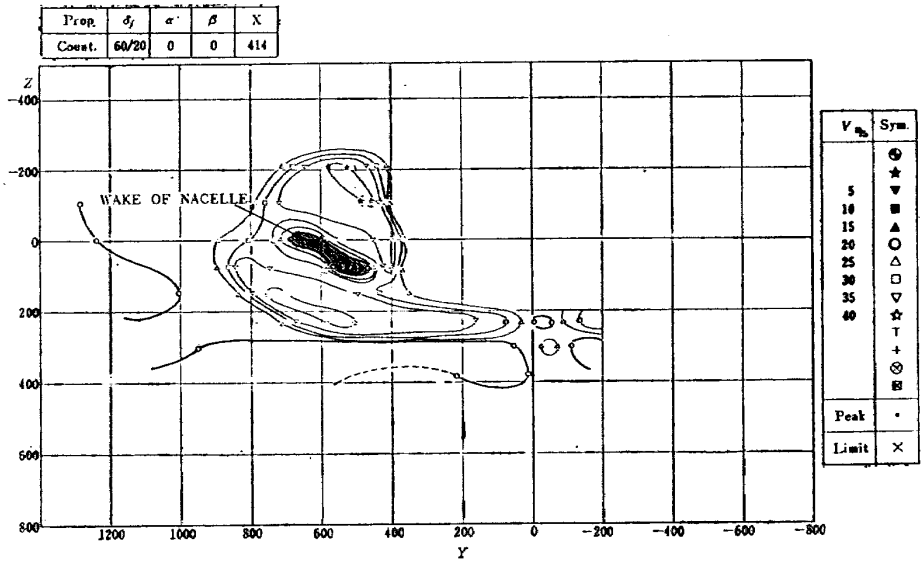

Fig. 13(a) Successive development of high speed region (sym. rotation), $X=414$ mm

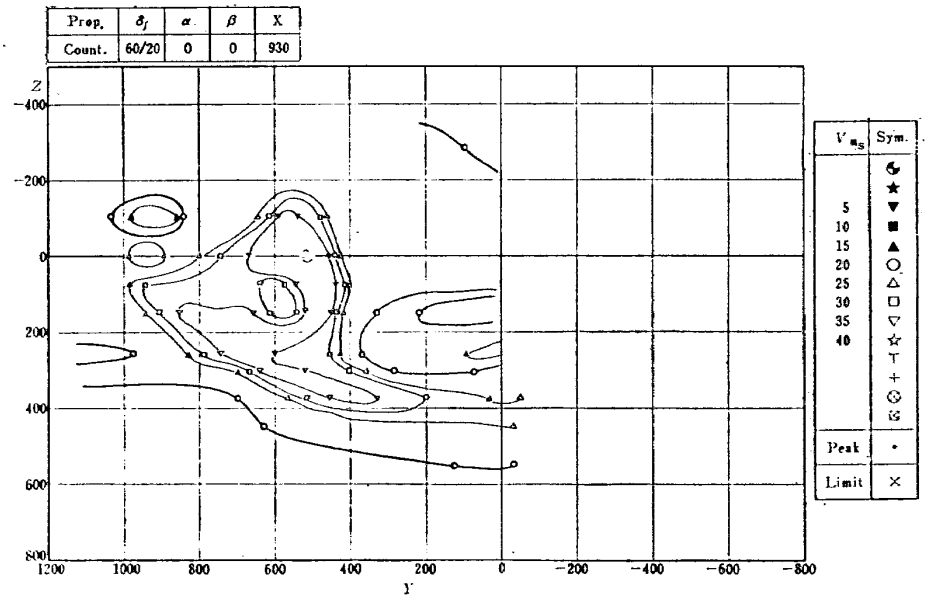

Fig. 13(b) (Continued), $X=930\frac{1}{8}$ mm

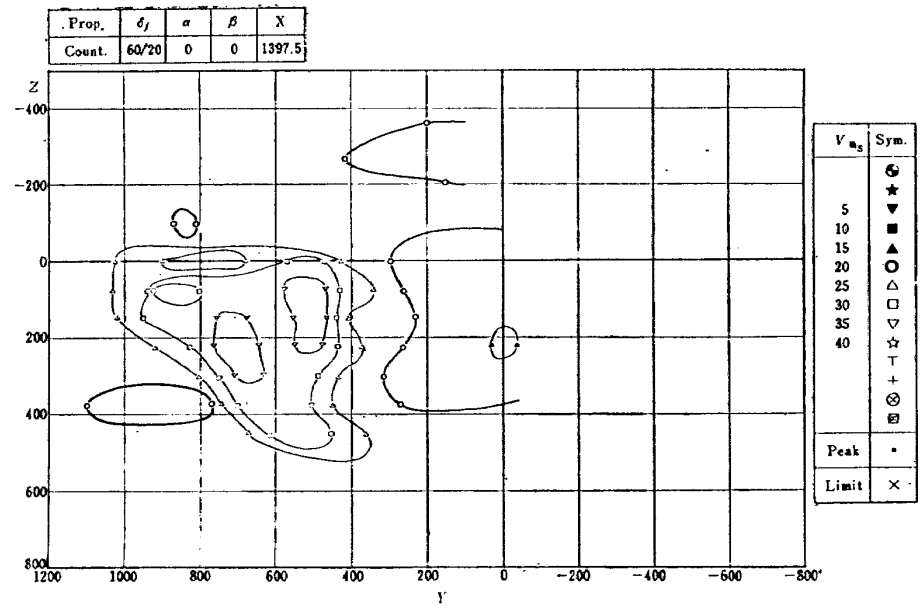

Fig. 13(c) (Continued), $X\fallingdotseq1400$ mm

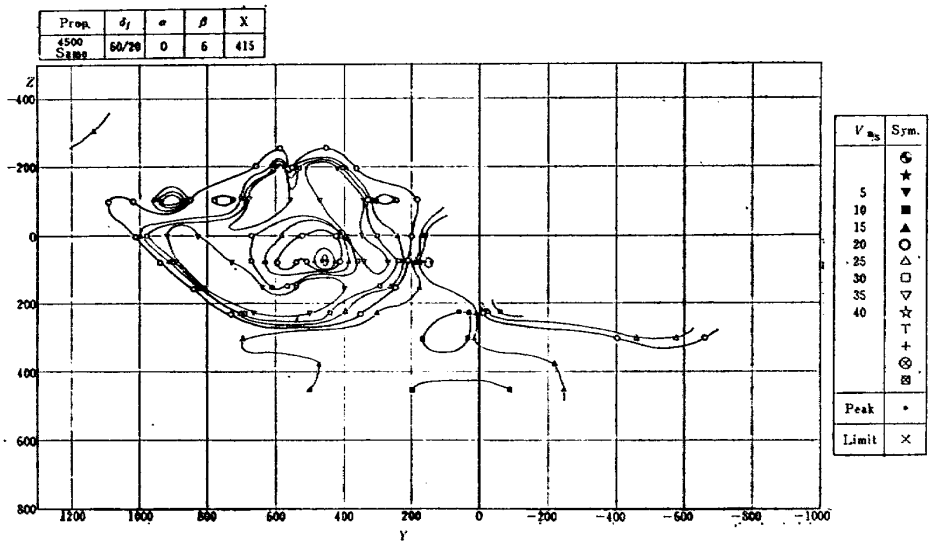

Fig. 14(a) Successive development of high speed region (same rotational direction), $X=415$ mm

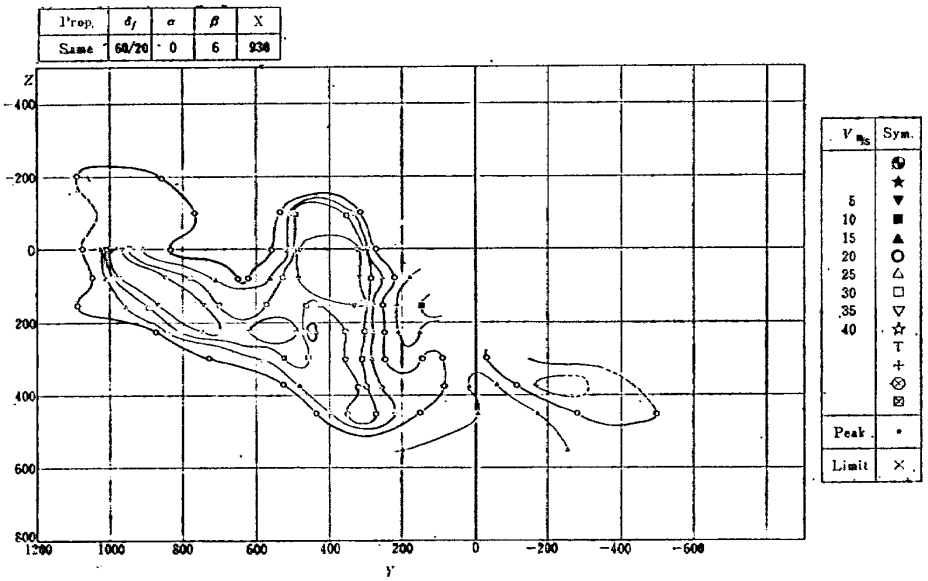

Fig. 14(b) (Continued), $X=930$ mm

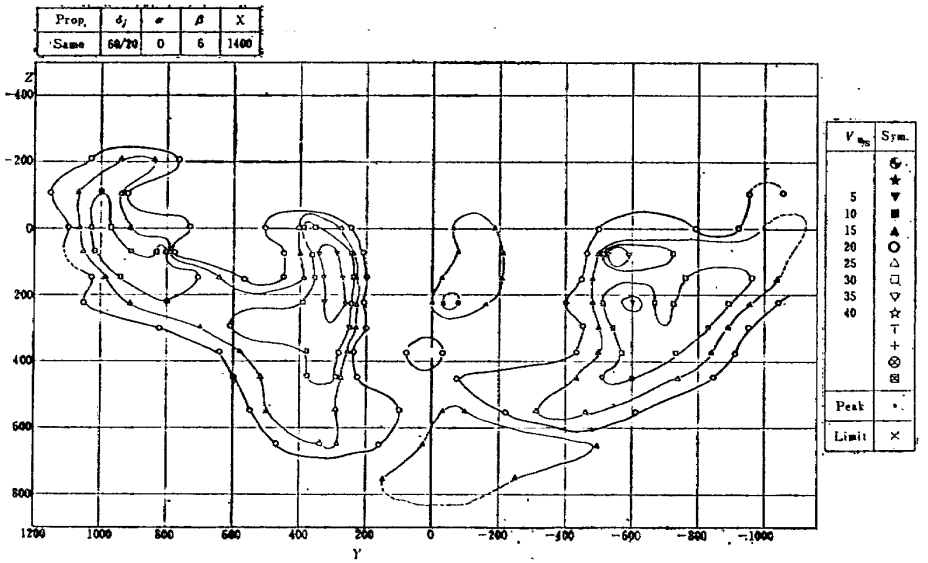

Fig. 14(c) (Continued), $X=1400$ mm

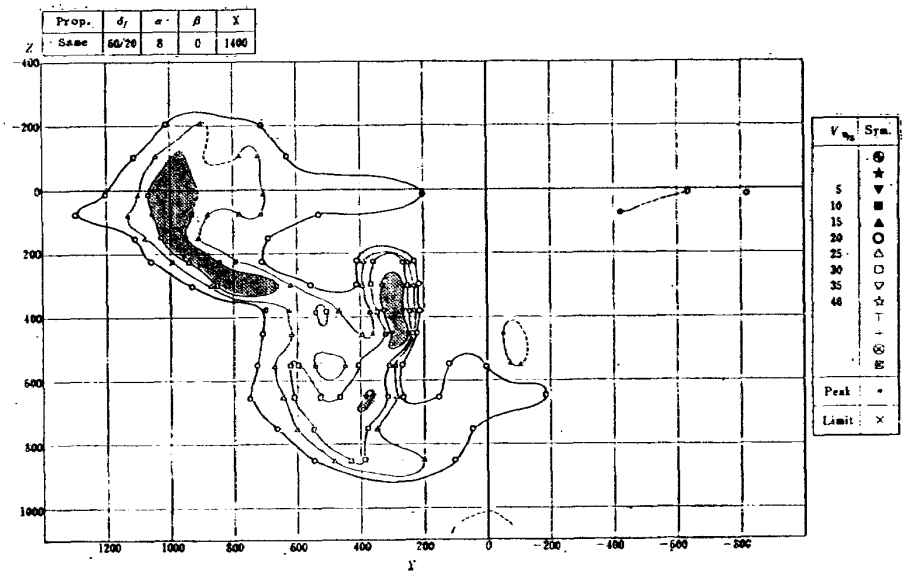

Fig. 15. Deformation of the high speed region corresponding to Fig. 11(c)

7. INTERNAL STRUCTURE AND DIEFUSION OF THE SLIPSTREAM

(1) In the Case of Clean Configuration (δ_f= 0 degree)

Generally speaking in this case, the region of the high speed sipstream has a nearly cylindrical shape. The velocity gradient in the shear layer of its boundary is steep. The thickness of the shear layer is comparatively thin. Then, the velocity distribution is nearly flat in its cross section, except for the center part. In the center part of the cross section, there exists a low speed region which corresponds to the wake of the nacelle. Diffusion of high speed flow can be observed in the results of measurements. The area of the high speed region expands to some extent, and so does the low speed center area too, with flowing downstream. In the cylindrical high speed region, the circulating flow around its center is confirmed by the inspection of the data. This trend has been already discussed with reference to Fig. 10, in the section 6, in the case of symmetrical rotation. In the case of same rotational direction of propellers, we can also point out the circulating flow. Fig. 16 (a), (b) show us the distribution of ε and σ in the case of Fig. 9. The trend of circulating flow due to propellers can be found. Some-

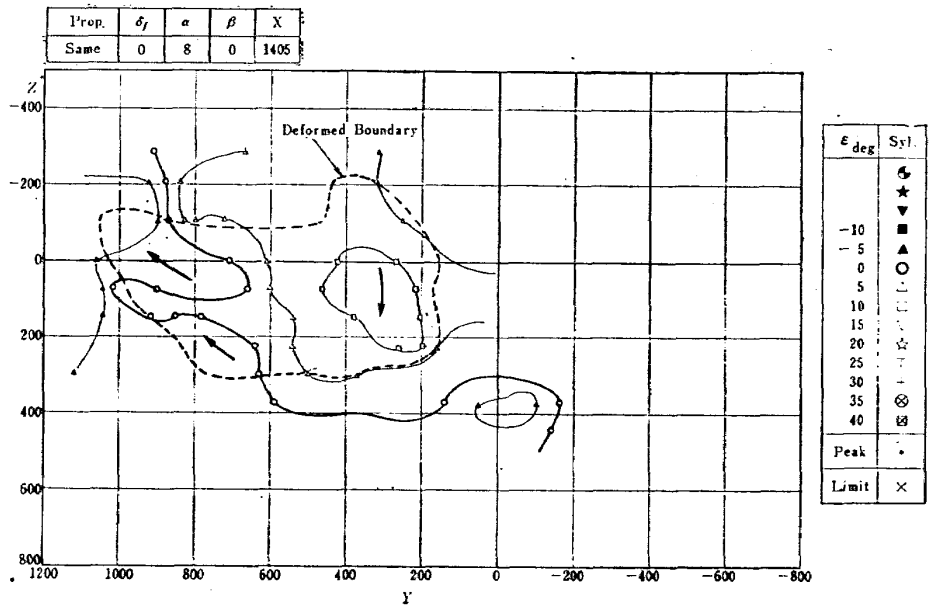

Fig. 16(a) Down wash field (in the case of Fig. 9)

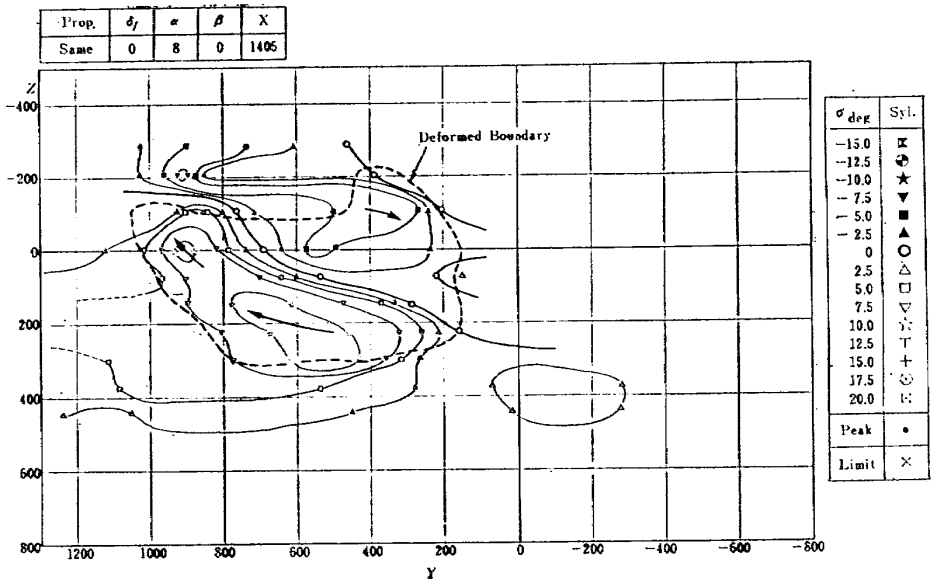

Fig. 16(b) Side wash field (in the case of Fig. 9)

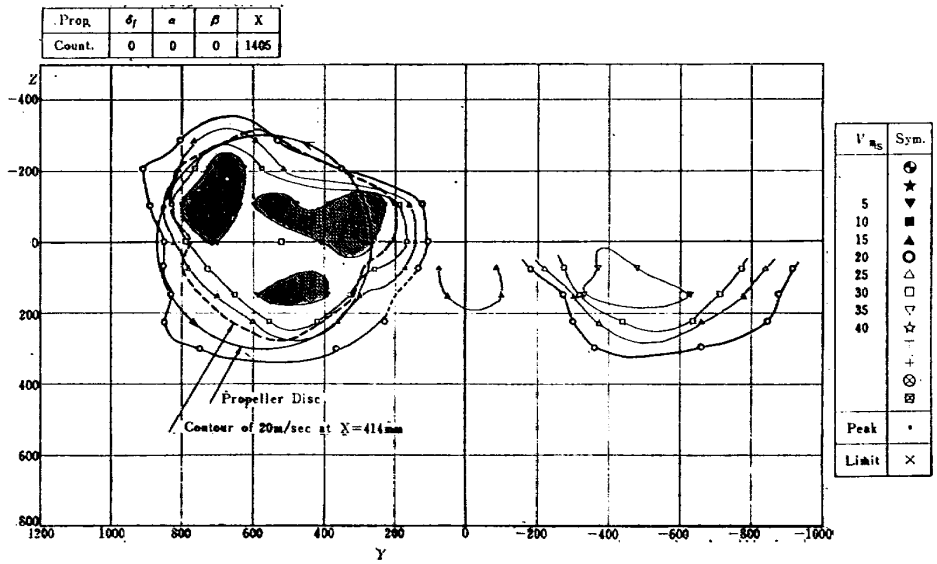

Fig. 17. Diffusion and development of the Slipstream (cf. Fig. 7)

times a few peaked region of the velocity field appear in the cylindrical field with the progress of the diffusion, as it can be seen in Fig. 17. But the cylinder itself does not exhibit a marked horizontal movement (in Y direction).

(2) In the Case of Flapped Configuration (δ_f=60/20 degrees)

In this case, as already explained in the section 6. (2), there arise severe transitions of the wake field. The mechanism of the transitions is far from analysis. But the trends of those complicated flow field can be pointed out. At the station of X=400, the flattened wake of the nacelle separates the two regions of the upper and lower high speed cores (see Fig. 13 (a)). Instead of the circulatory cylindrical flow of the previous case (δ_f=0 degree), rapid diffusion and rotation of the slipstream take place successively. But in each separated high speed region, the partially circulating flow is still observable. With reference to Fig. 13, the diffusion is supposed to be more rapid in the lower region (which past below the wing) than the upper region, because of its trend of extension.

(3) Increased Turbulence in the Slipstream

In the free stream, the turbulence level in $\Delta V/V$ is less than 1%. In the slipstream the velocity and turbulence are considerably higher than that of the free stream. Fig. 18 indicates the order of increased turbulence level in the slipstream. The more increased turbulence in the case of a flapped model can be seen. But the increment of turbulence due to the deflected flaps is not so remarkable compared with the influence of propeller.

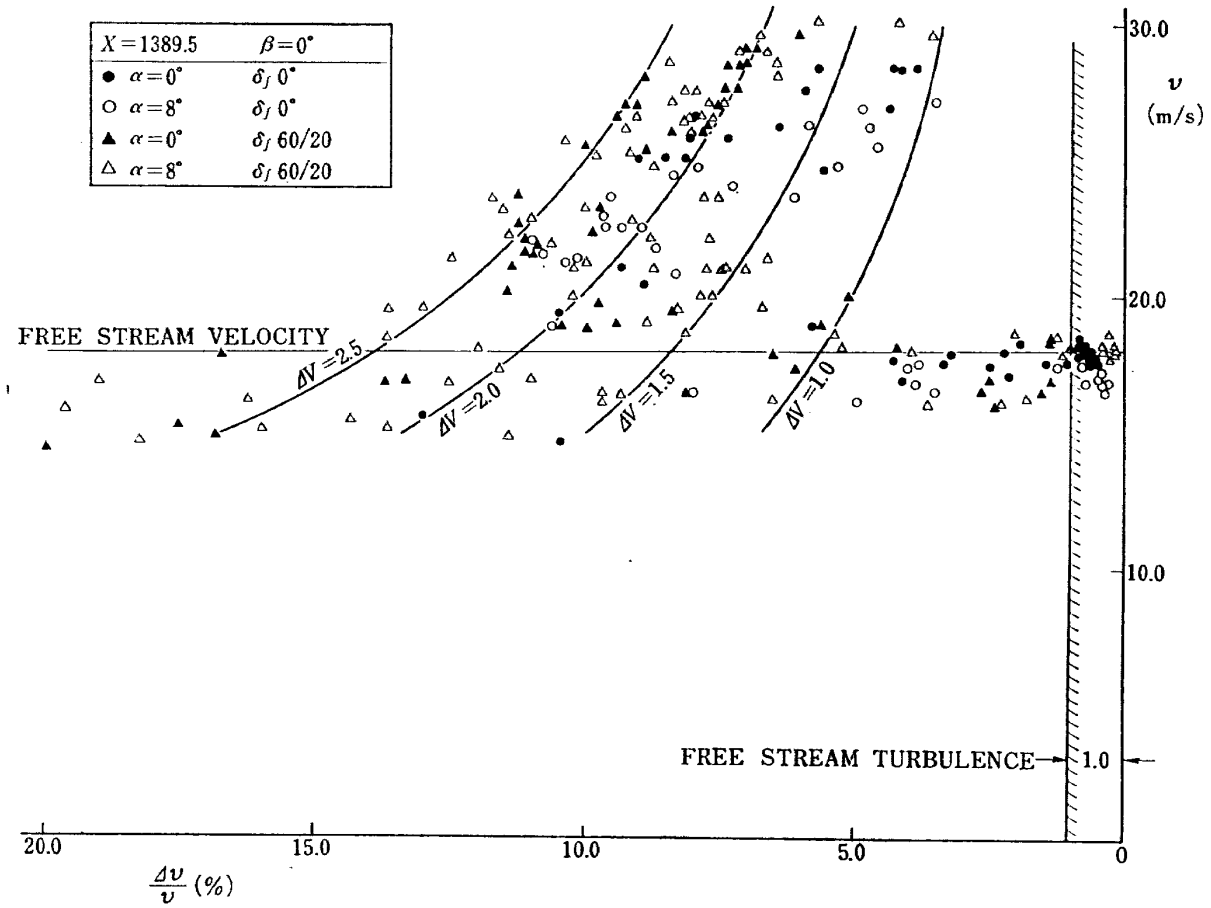

Fig. 18. Increased Turbulence level in the Slipstream

In Fig. 18 the region of low speed (less than the free stream velocity 18 m/sec.) and high turbulence level (more than 1%) may correspond to the wake region. The upper limit of the fluctuating frequency guaranteed by the tracking velocitymeter is about 0.2–0.3 cycle/sec.[3] On the other hand, hot wire anemometer used is guaranteed for the frequency higher than 2 cycle/sec. The questions may be arisen about the frequency of fluctuating velocity in our measurements, and about the steadyness of the flow field. However, in the cases of collected data in Fig. 18, the marked flow separation cannot be observed on the wing surface. And the distribution of the turbulence level has a similar type of plateau just as the velocity distribution, across the slipstream. Furthermore, the tracking senser of the velocitymeter (pitot head) does not exhibit the marked oscillation in the wake field, except for the boundary of the slipstream where a thin shear layer exist. Then, it is convincing that the rotating propeller increases the turbulence, and that the measured flow field may be at least quasi-steady. The increased turbulence may affect the wing char-

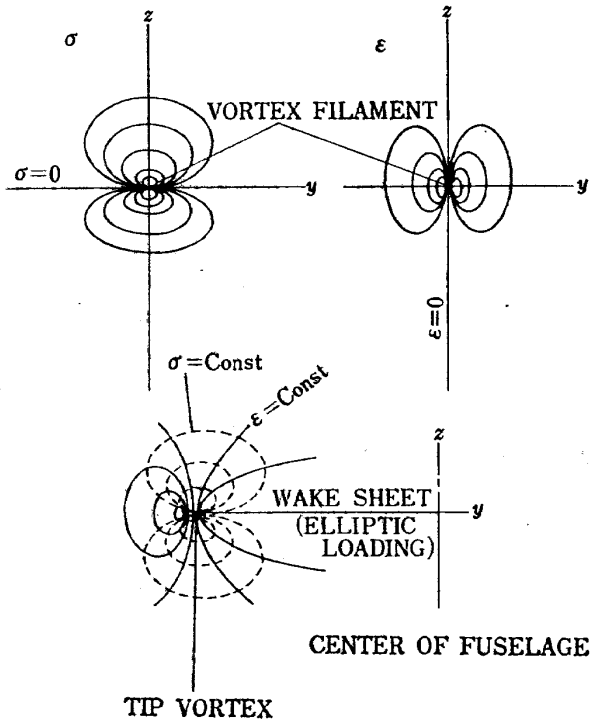

Fig. 19. Contour maps of the vortex filament and wake sheet

acteristics and the wake flow, but further discussion is out of our aims.

8. WING TIP VORTEX AND ROLLING UP OF THE WAKE SHEET

The contour maps are less intuitive compared with such representations as the velocity vectors in Fig. 6. However, for the quantitative analysis of the flow field, and for the inspection of the correspondence between the actual wake field and the model of flow patterns of the imaginable vortex systems, the contour maps may be more useful. Then, we consider some of the typical patterns of contour maps with reference to the vortex systems.

At first we suppose a single vortex filament perpendicular to the vertical plane of wake survey. The contour maps of ϵ and σ must be as will be seen in Fig. 19. If we suppose the vortex wake sheet instead of the vortex filament, the contour maps must be as the last sketch of Fig. 19. For example, in our results of Fig. 20 we can see the similar arrangement of contour lines corresponding to the tip vortex.

With the considerations explained above, we can point out the position of the tip vortex readily in the contour maps. In all cases of our results, the lateral position of the tip vortex is about $Y \fallingdotseq 800 \sim 900$ mm. In some cases the tip vortex is joined in the region of the slipstream, but the circulating flow around the tip vortex is still definitely observed. Fig.

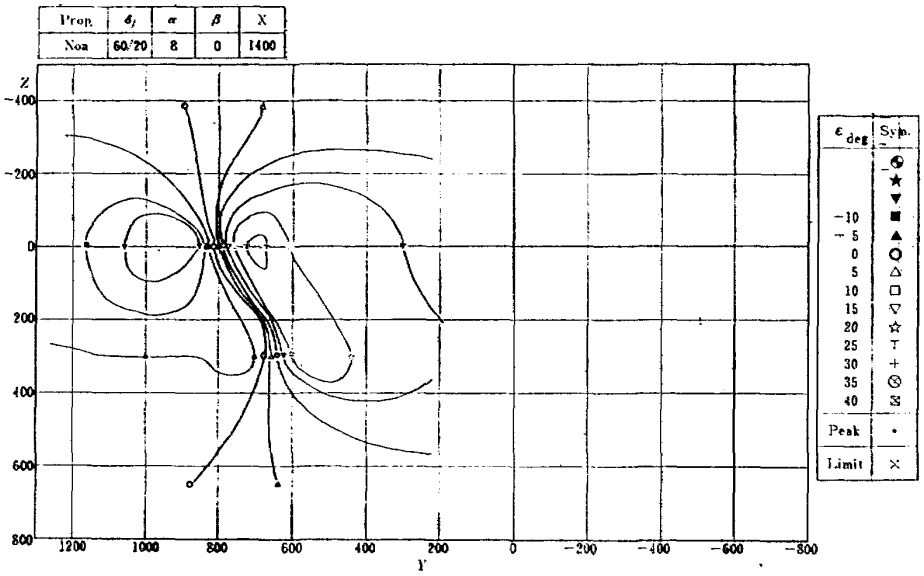

Fig. 20(a) Down wash field of tip vortex (power off condition)

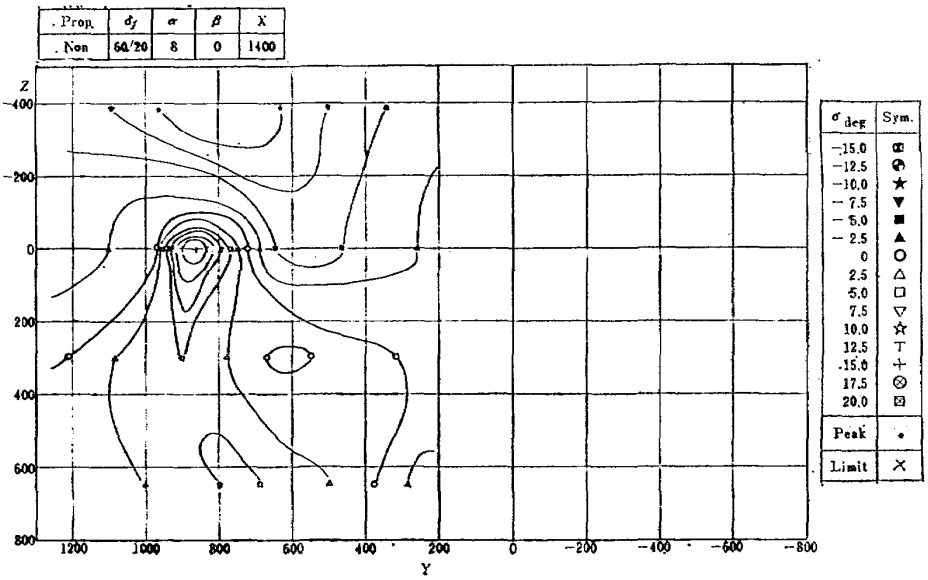

Fig. 20(b) Side wash field of tip vortex (power off condition)

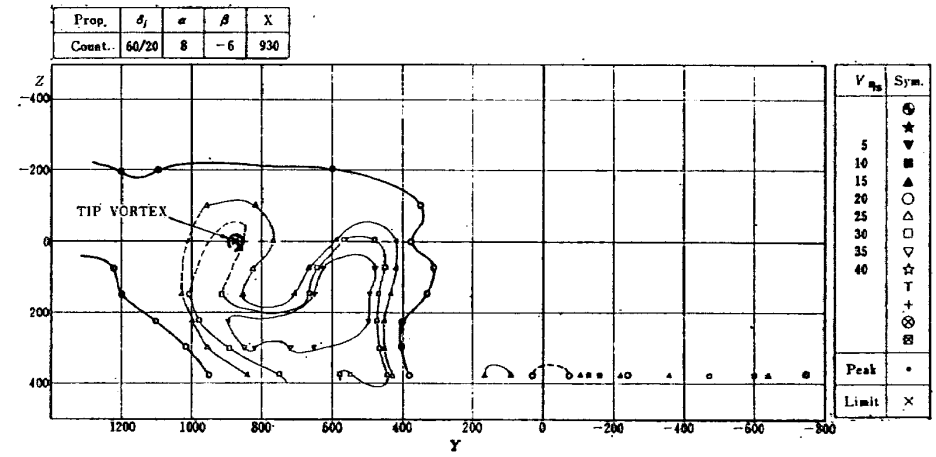

Fig. 21(a) Tip vortex involved in the high speed region (velocity field)

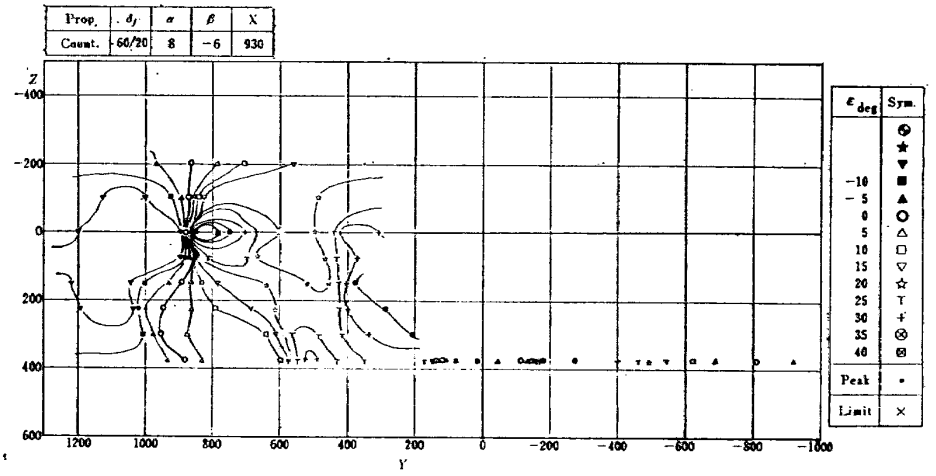

Fig. 21(b) (Continued) (down wash field)

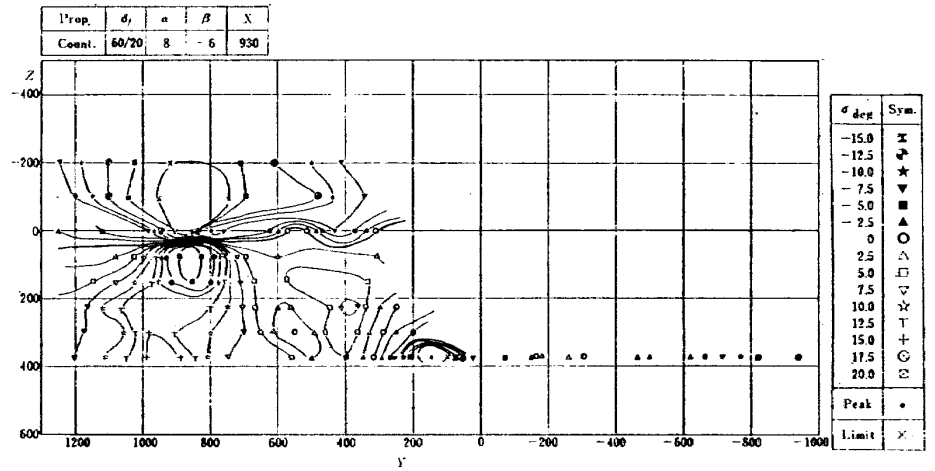

Fig. 21(c) (Continued) (side wash field)

21 is one of the examples of these cases.

The movements and rolling up of these tip vortices are not so obvious in the measurements. The position of the wake vortex sheet is not clear, because of the existence of the slipstream. But it is supposed that the wake sheet may be on a line joining the tip vortex, and the center of the nacelle wake with inner edges of the stretched slipstream cross section.

Anyway, in our problem it must be inadequate if we assume the usual wake sheet, because the nonuniformity and complexities are severe in the flow field. Now, instead of assuming the usual wake sheet, we have to give our attention to the mutual movements of the vortex systems in the wake field. In the fol-

lowing sections we shall discuss the several nonlinearities in the aerodynamic coefficients of the STOL airplane model, with attention to the movements of the vortex systems in the wake field.

9. ON THE NONLINEAR AERODYNAMIC CHARACTERISTICS OF POWERED MODEL

(1) Longitudinal Characteristics

The longitudinal static instability was presented in our previous reports.[1),2)] It was considered that the instability might be due to the ineffectiveness of the tail plane. For example Fig. 22 shows these results. In our present measurements the supposed position of the mid. tail plane is about $X=1{,}230$, $Z=-175$ (mm) at $\alpha=0$ degree. At $\alpha=8$ degrees the position is about $X=1{,}260$, $Z=16$ (mm). The length of semispan of the tail plane is 458 (mm). In consideration of such dimensions, we must inspect the down-wash angle in the tail plane position. The contour maps of the down wash field are given in Fig. 23(a), (b), (c), (d). Then, we can see the increase of down wash angle with increasing angle of attack. At $\alpha=0$ degree, the down wash angle is about 15–20 degrees, but it becomes about 20–30 degrees when α is increased to $\alpha=8$ degrees, at the position of mid. tail plane. Therefore, it is conceivable that the static longitudinal instability depends mainly on the variations of the down wash field around the tail plane. In other words, the increase of down wash angle in the tail plane is of the same order as the increase of the angle of attack, in the unstable region of C_m. Thus, the

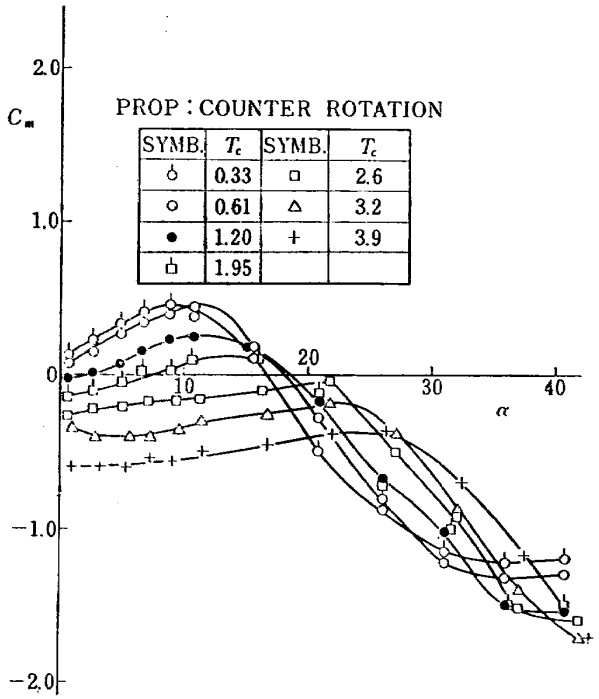

Fig. 22. Variation of C_m. ($\delta_f=60/20$ degrees, blade pitch angle 20 degrees, low tail, reference 2); complete model

ineffectiveness of the tail plane and the instability must arise in these conditions.

On the other hand, the down wash angle is less in the upper region of the tail plane. Then, if we take the higher tail position, the pitching moment of the model must be more negative (nose down). The related results of our previous report are given in Fig. 24. This trend can be supported by Fig. 24.

The possibility of precise estimation of the tail contribution may be still doubtful, because of the complexities of the wake field.

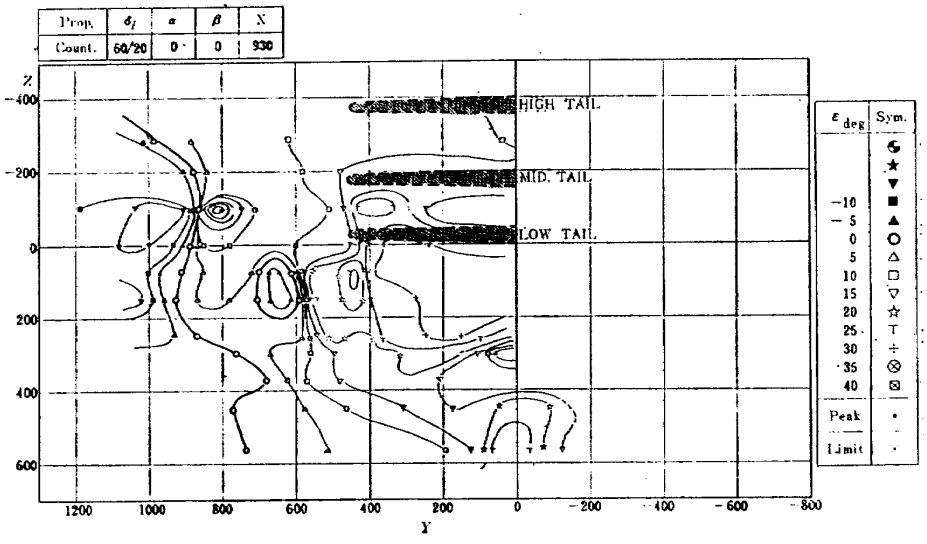

Fig. 23(a) Down wash field near the tail position ($\alpha=0$, $X=930$ mm)

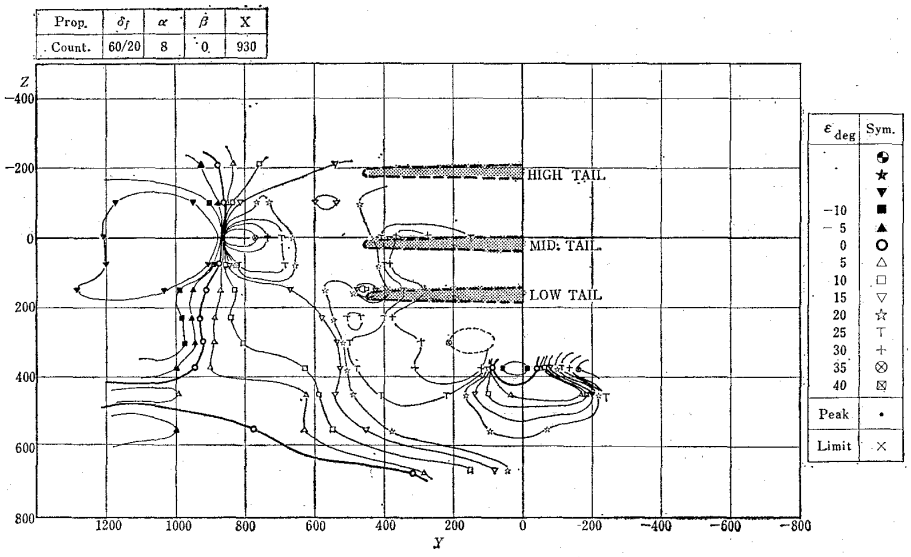

Fig. 23(b) (Continued) (α=8 degrees, X=930 mm)

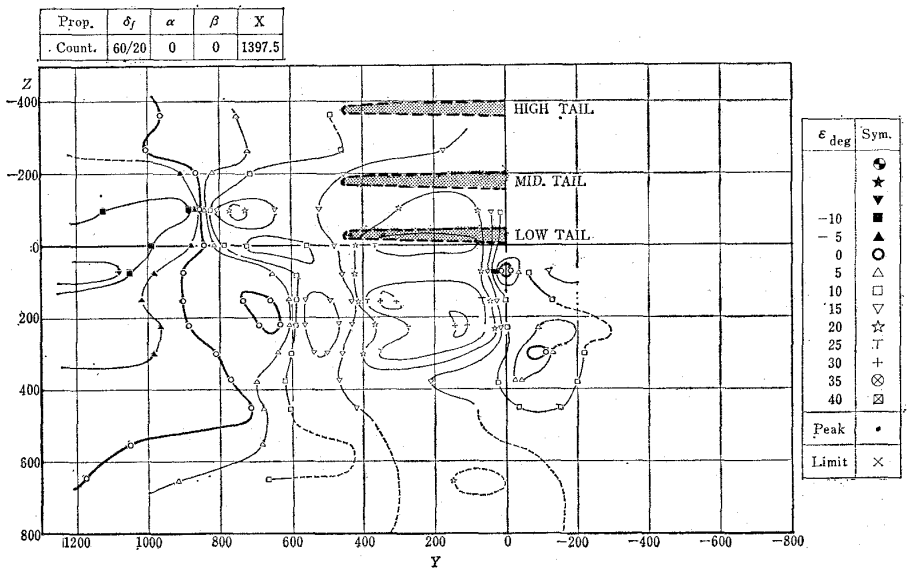

Fig. 23(c) (Continued) (α=0, X≒1400 mm)

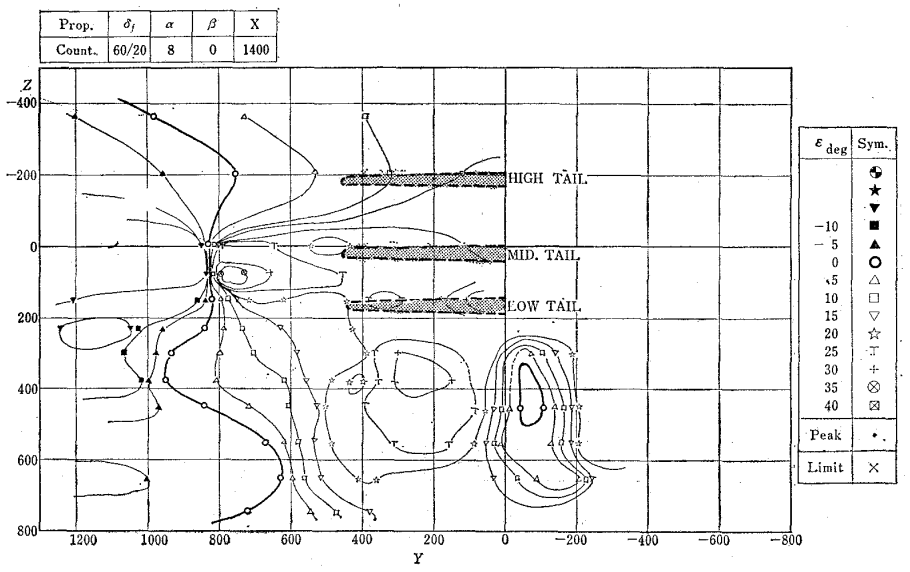

Fig. 23(d) (Continued) (α=8 degrees, X≒1400 mm)

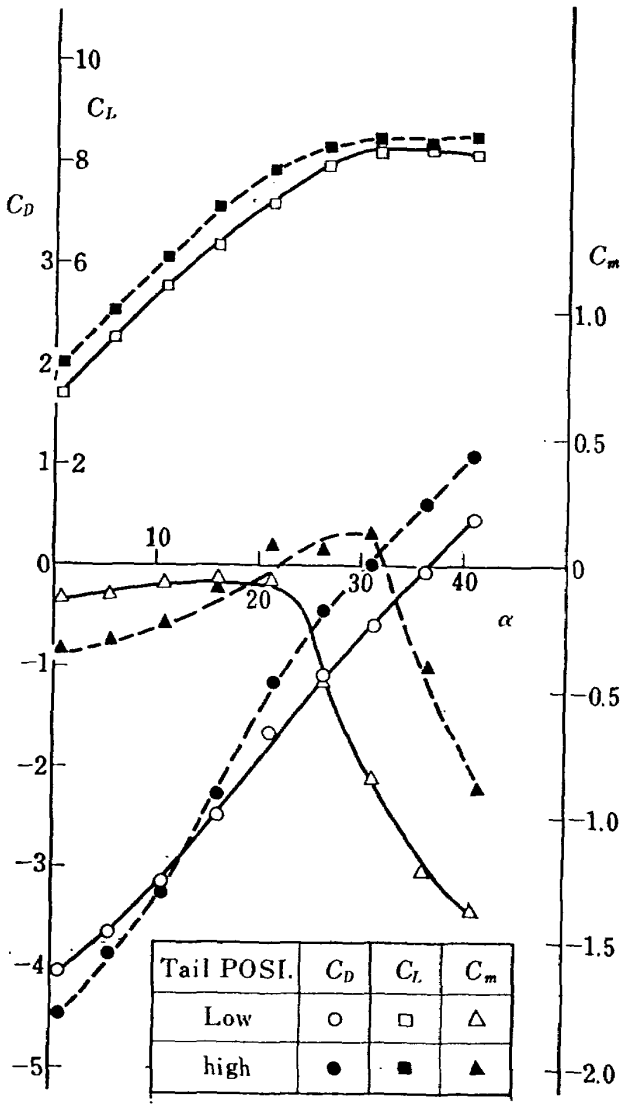

Fig. 24. Effects of tail position (δ_f=60/20 degrees, reference 2)

(2) Lateral Characteristics (with the symmetrical rotation of the propellers)

In view of our previous results, one of the nonlinear stability derivatives is the side slip derivative $C_{l\beta}$. Its nonlinearity arises at the higher angles of attack. The mechanism of this nonlinearity is usually explained in taking acount of the lateral movements of the slipstream due to side slip. Then, we shall discuss the rest of nonlinearities.

Even in the cases of symmetrical propeller rotation, there still remains the nonlinearity of $C_{n\beta}$. It arises when α is small, and in the range of β=5~−5 degrees, and only in the flapped configurations. Fig. 25 is the related data of our previous report. The results of our present measurements are given in fig. 26 (a), (b), (c), confirming our previous results. In Fig. 26(a) (α=0.1 degrees, δ_f=0 degree; clean configuration), we can see the linear variation of aerodynamic coefficients. But in Fig. 26(b) (α=1.0, δ_f=60/20 degrees; flapped configuration), we see the similar nonlinearities of C_y and C_n evidently even in such a tailless configuration. In Fig. 26(c) where α is increased (α=9.4 degrees), the prescribed effects are more less observable.

Now, we should turn our attention back to the corresponding wake field i.e. to the contour maps. Generally speaking, at first we suppose the symmetrical arrangement of the vortex systems and contour maps as given in Fig. 27. However, the results of our measurements do not indicate such a strictly symmetrical arrangement. There arises an asymmetric flow field as already pointed out. Across the plane of symmetry, the flow region of each side protrude alternately from each side. Consequently the arangement of vortex systems are less symmetrical near the plane of symmetry. For example, Fig. 28 shows us the alternate change of flow direction of side wash in the plane of symmetry. These results suggest that the symmetrical flow may be rather unstable in the actual cases especially near the plane of symmetry. In the schematic sketch of Fig. 29(a), first we suppose the symmetrical pair of vortices A, B beside the plane of symmetry. But in taking account of those results, it seems to be unlikely that such a symmetrical arrangement of A, B can be a stable one.

On the other hand, in the case of slight sideslipping conditions, the flow pattern seems to be settled like the sketch of Fig. 29(b). The fuselage seems to be involved in the vortex B, and the circulation seems to be arisen around the fuselage. Thus, in the down wash field of the wing, the additional force and moment must be experienced by the fuselage. We can suppose that those additional force and moment are the possible sources of the prescribed nonlinearity. The corresponding contour maps are given in Fig. 30. Although it is something like the diagnostics to find out the vortical flow patterns corresponding to the vortex systems sketched in Fig. 29(b), we can indicate such patterns in the contour maps (see Fig. 30). If the sign of β is reversed, the flow pattern is also reversed. For the inspection, reader is referred to Fig. 31 and Fig. 32. In these figures the reversed direction of the alternate distribution of side wash can be seen in the plane of symmetry. At the higher

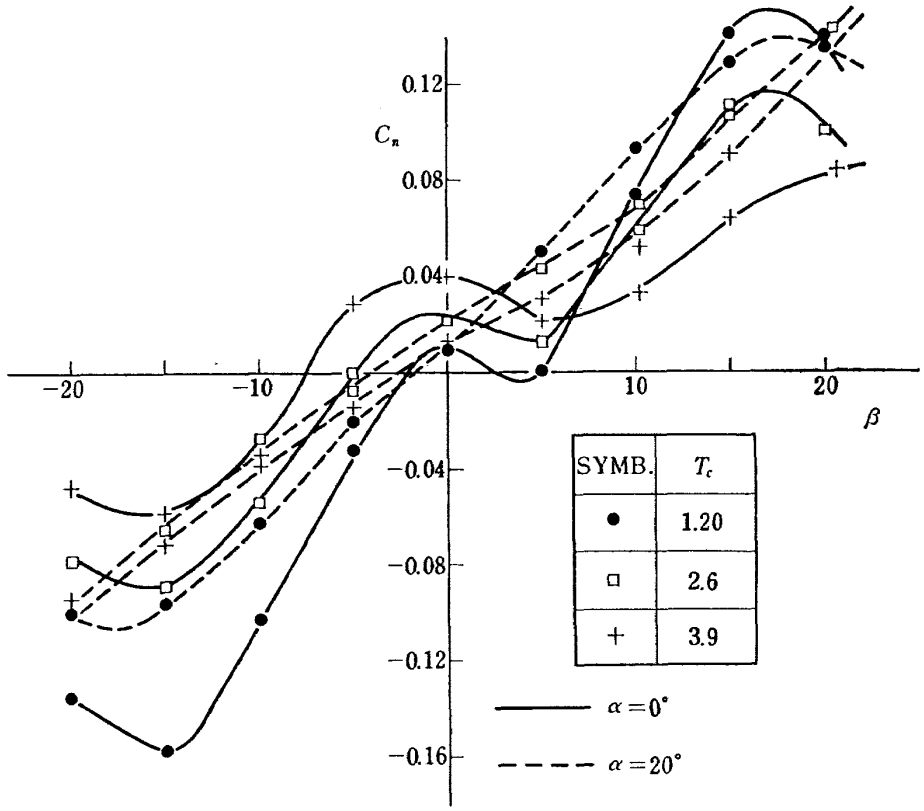

Fig. 25. Nonlinear variation of C_n (δ_f=60/20 degrees, reference 2); complete model

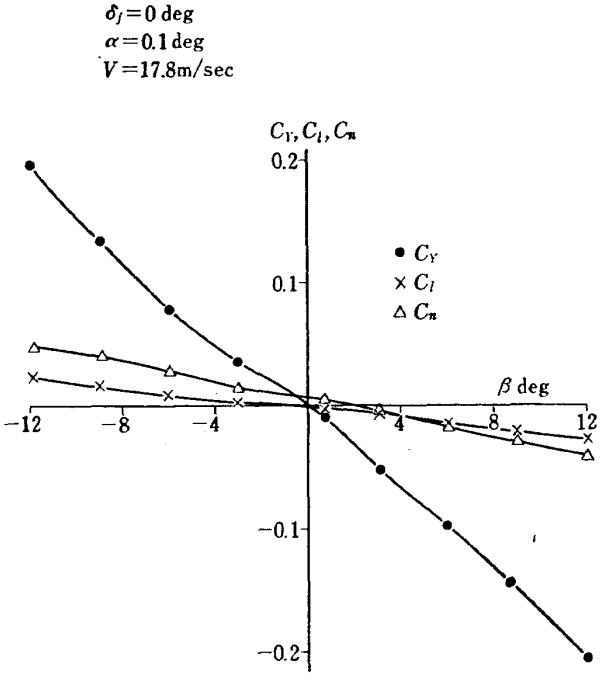

Fig. 26(a) Lateral characteristics (symmetrical rotation); tailless model

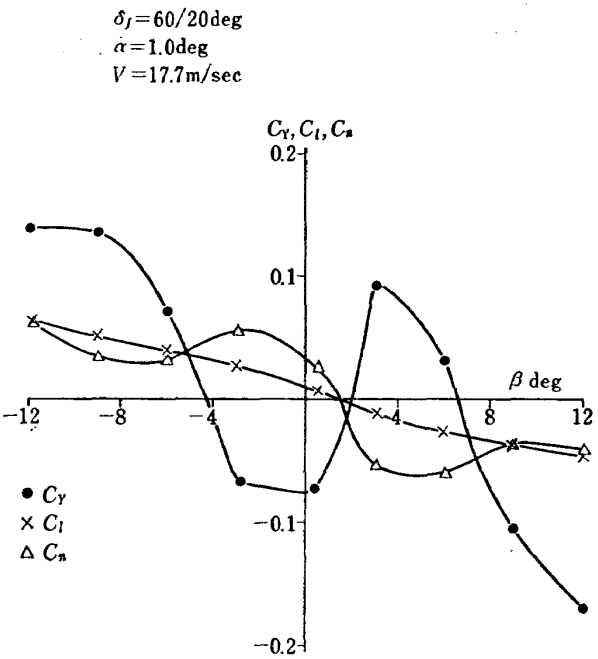

Fig. 26(b) Lateral characteristics (symmetrical rotation); tailless model

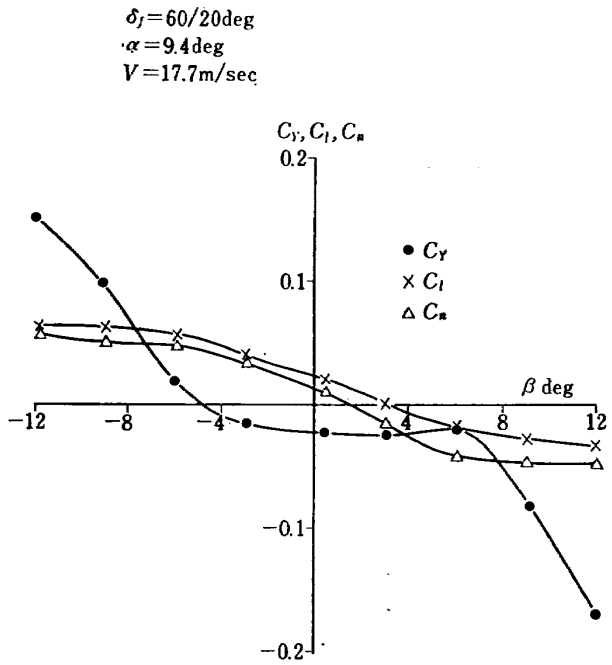

Fig. 26(c) Lateral characteristics (symmetrical rotation); tailless model

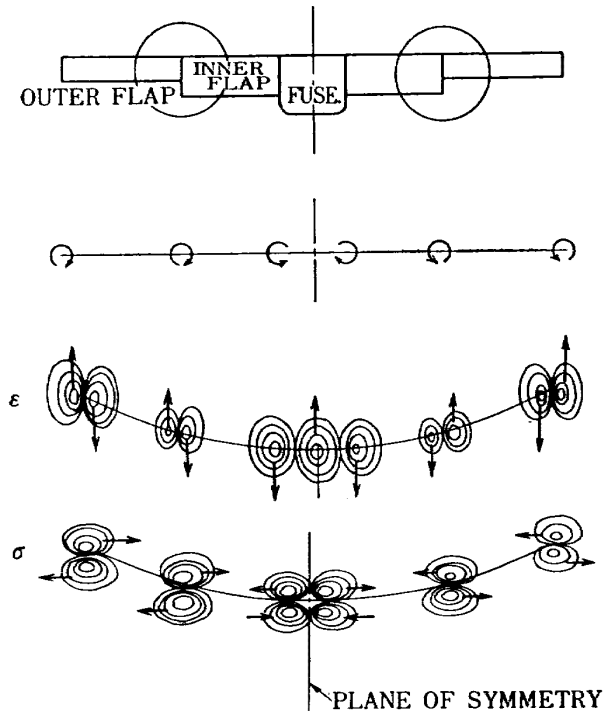

Fig. 27. Model of flow pattern in the symmetrical flow field

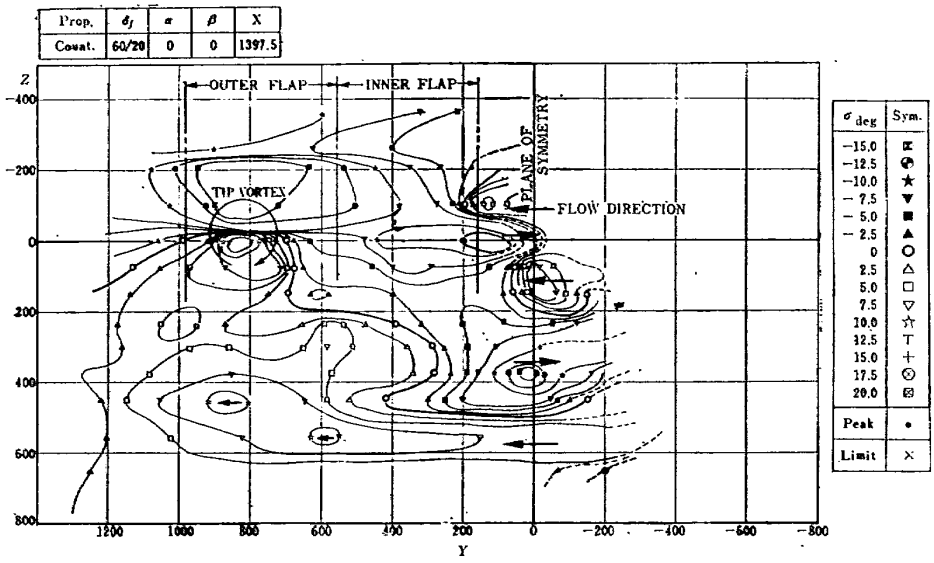

Fig. 28. Alternate direction of side wash in the plane of symmetry (cf. Fig. 27)

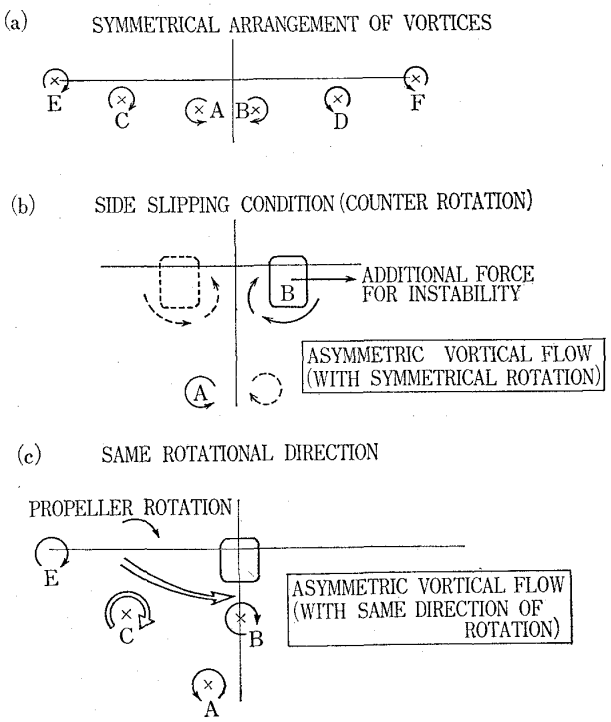

Fig. 29. Model of flow pattern in the asymmetrical flow field

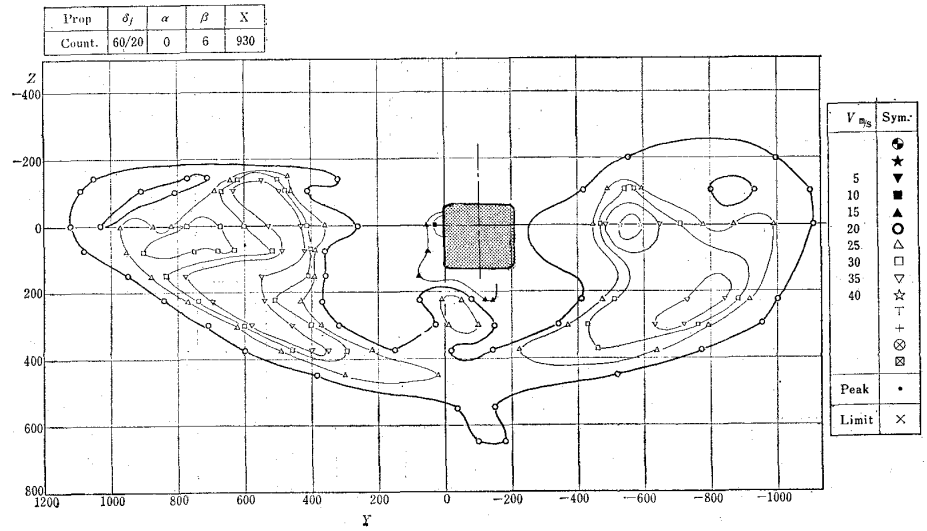

Fig. 30(a) Flow pattern of the slight side slip condition (velocity field); $X=930$ mm

Remarks: This mark represents the existence of vortical flow corresponding to Fig. 29(a), in the following figures.

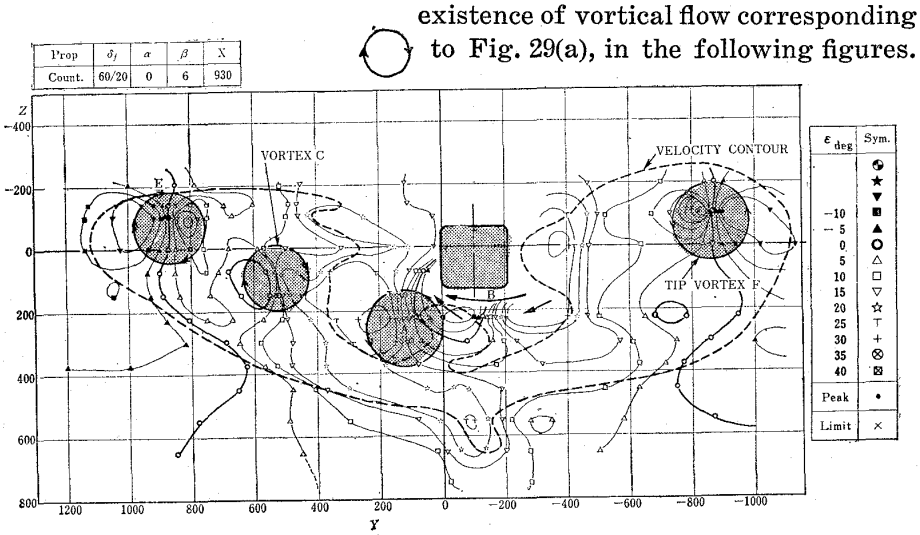

Fig. 30(b) (Continued) (down wash field); X=930 mm

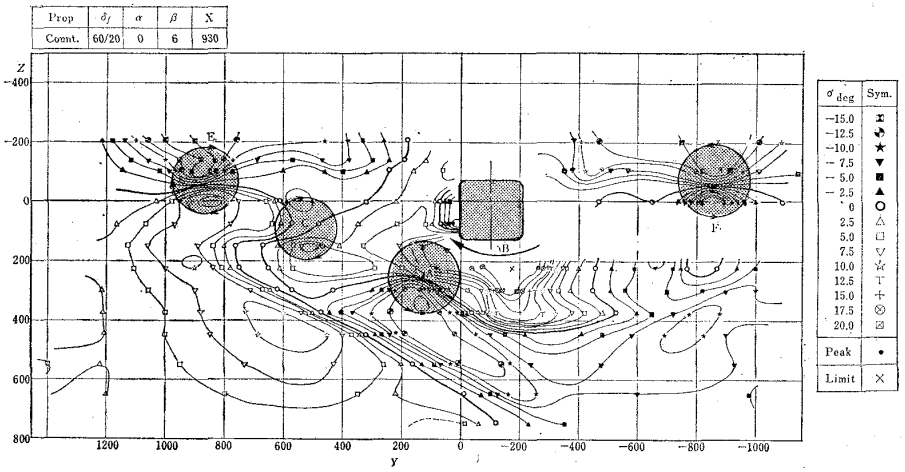

Fig. 30(c) (Continued) (side wash field); X=930 mm

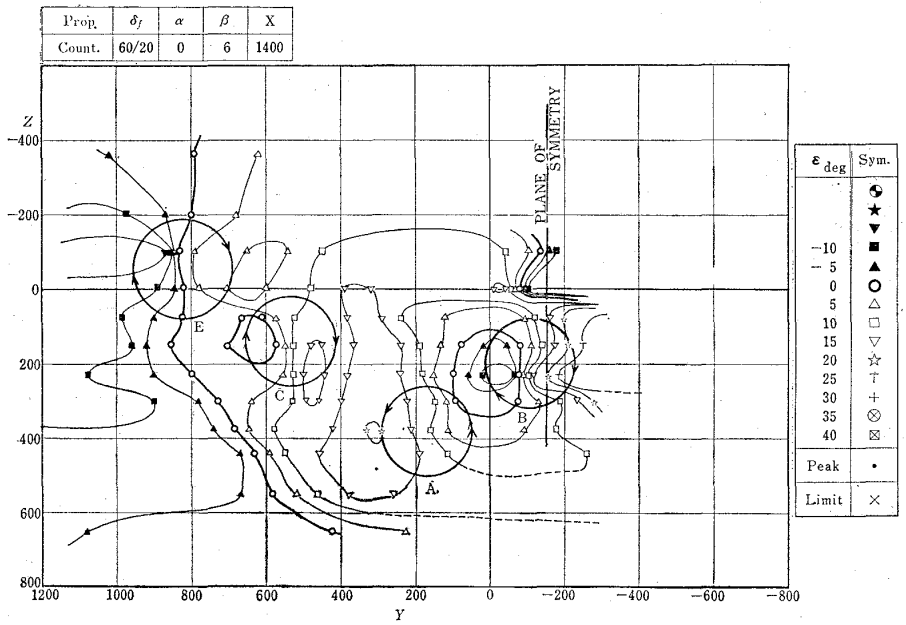

Fig. 31(a) Flow patten of the slight side slip condition (down wash field); X=1400 mm, β=6 degrees α=0

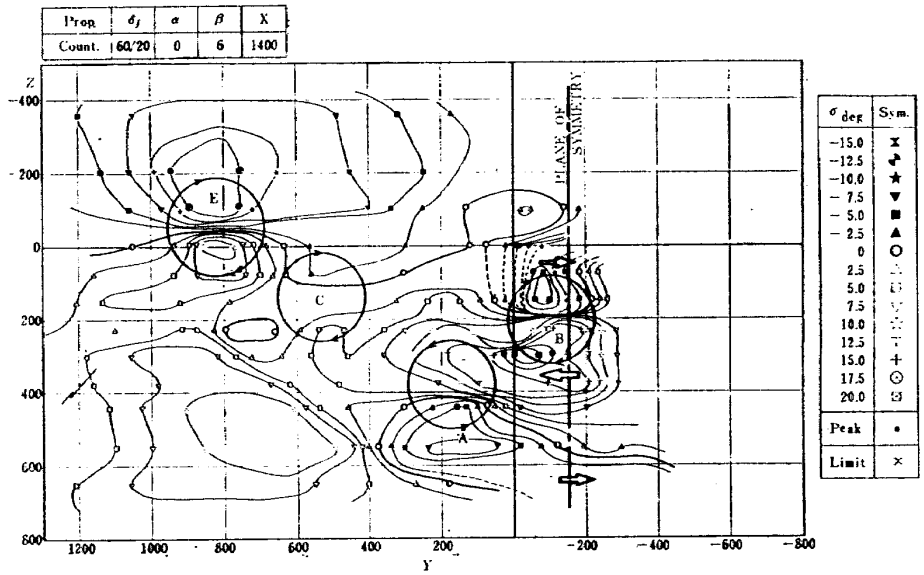

Fig. 31(b) (Continued) (side wash field); X=1400 mm, β=6 degrees, α=0

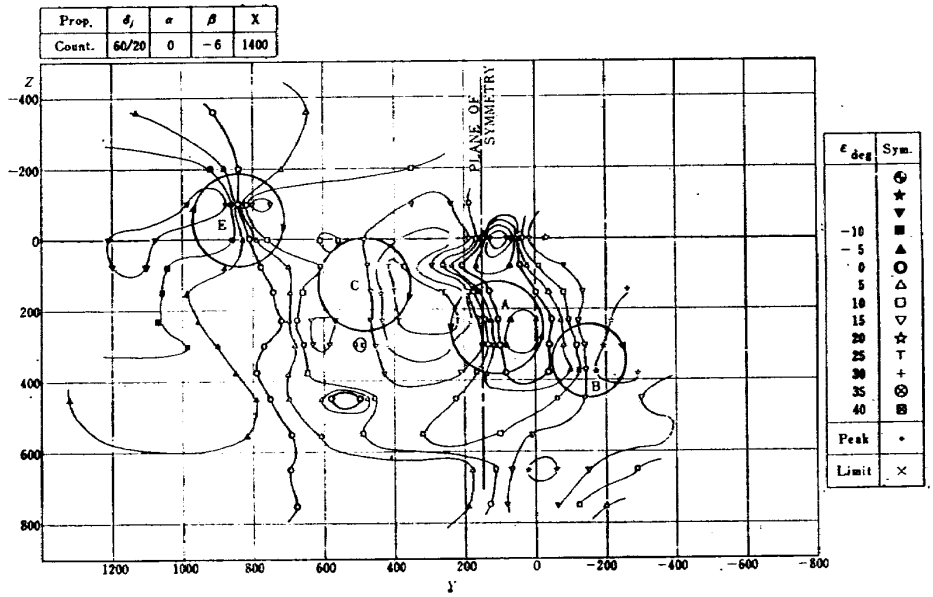

Fig. 32(a) Flow pattern of the slight side slip condition (down wash field); X=1400 mm, β=−6 degrees, α=0

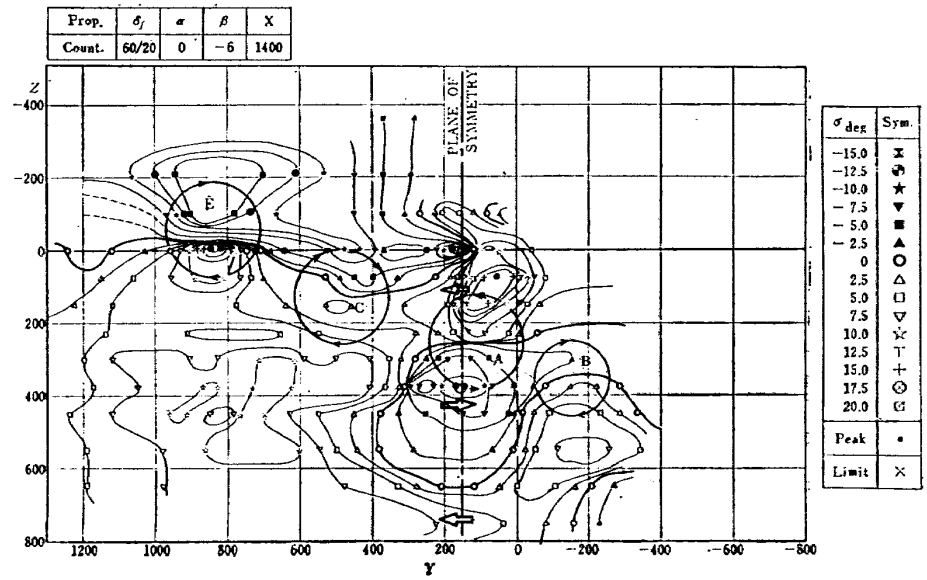

Fig. 32(b) (Continued) (side wash field); X=1400 mm, β=−6 degrees, α=0

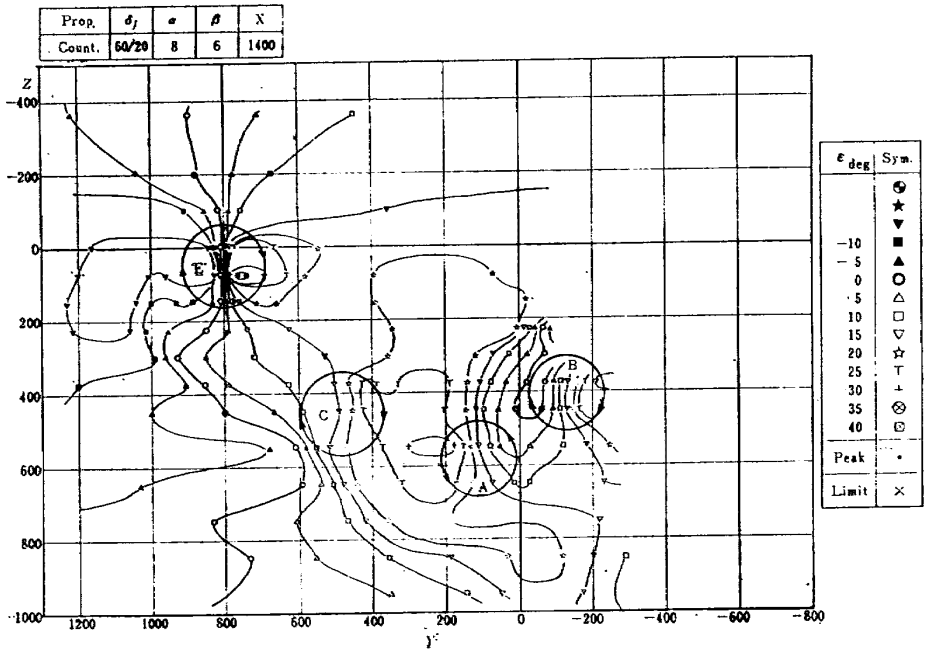

Fig. 33(a) Flow pattern of the sligh side slip condition (down wash field); $X=1400$ mm, $\beta=6$ degrees, $\alpha=8$ degrees

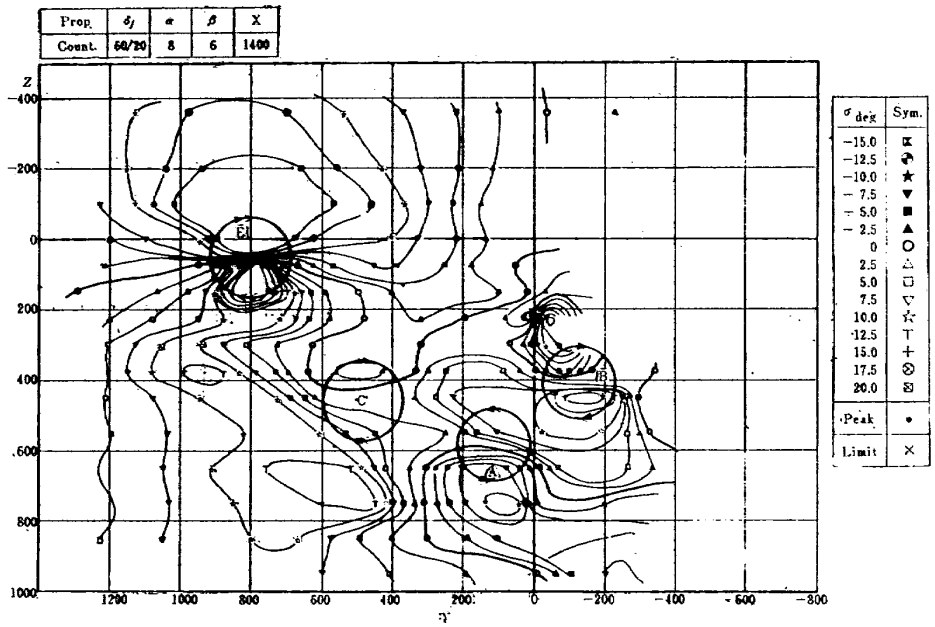

Fig. 33(b) (Continued) (side wash field); $X=1400$ mm, $\beta=6$ degrees, $\alpha=8$ degrees

angles of attack, probably the vortical flow around the fuselage may be degenerated, and the nonlinearity may fade away. About this argument, reader is referred to Fig. 33. In Fig. 33 ($\alpha=8$ degrees), we can also find out the vortical flow corresponding to the vortex B of Fig. 29(b), but it is more less remarkable compared with the case of Fig. 31. The prescribed explanation of additional force and moment, which is deduced from the wake survey, is feasible for the interpretation of the force test results (Fig. 25 and 26) of the nonlinear variations of C_y and C_n.

(3) Lateral Characteristics (with the same rotational direction of the propellers)

Now, we shall discuss the nonlinearity of C_n which arises in the case of the same rotational direction of propellers. In this case it was indicated in our previous results that the asymmetric yawing moment might arise intensively even in the case of $\beta=0$ degree. The results are given in Fig. 34, for example. For the confirmation of our previous results, the data of our present measurements are pre-

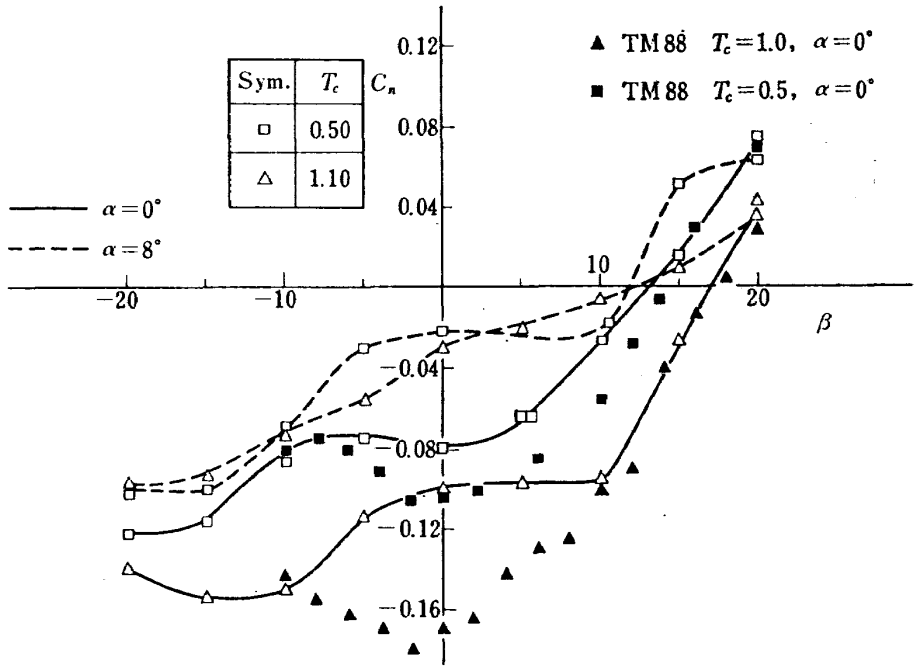

Blade pitch angle: 8 degrees, Prop: Same direction

Fig. 34. Nonlinear variation of C_n (δ_f=60/30 degrees, references 2); complete model

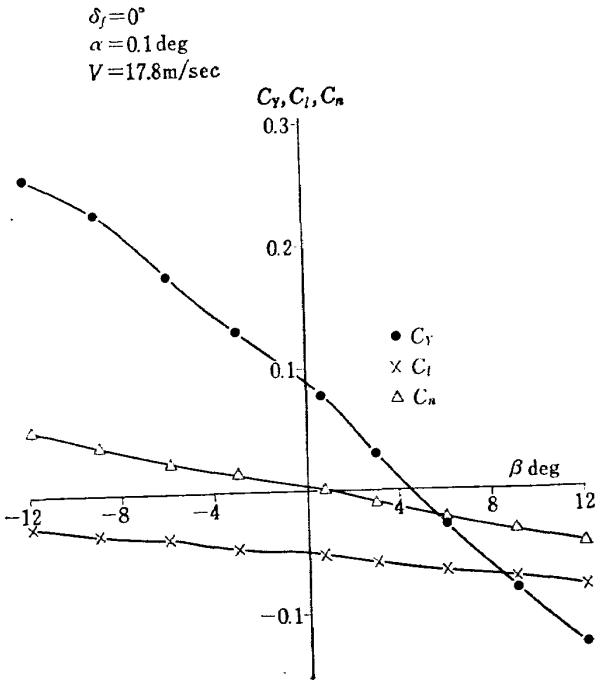

Fig. 35. Lateral characteristics (same direction of rotation); tailless model

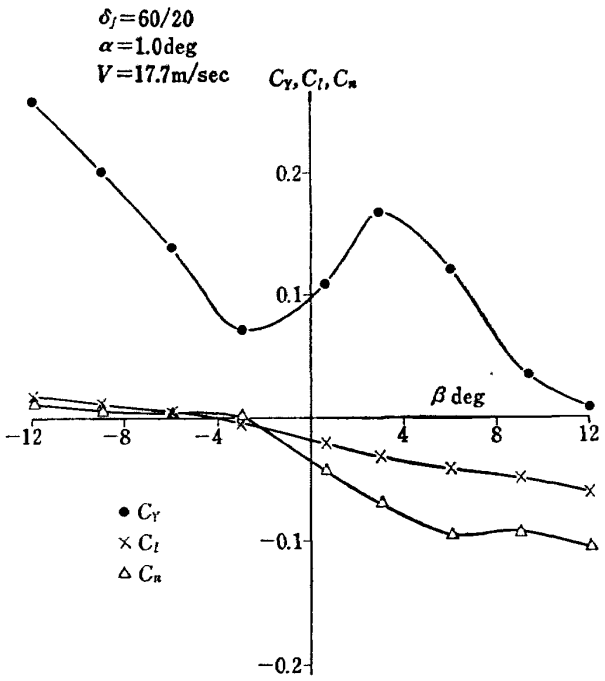

Fig. 36. Lateral characteristics (same direction of rotation); tailless model

sented in Figs. 35 and 36. In the case of clean configuration (Fig. 35), the marked shift in C_y and C_l are observed, compared with Fig. 26(a). But there is no apparent shift in C_n. These trends are also verified in our previous report in the case of the complete model. Therefore, it is supposed that these shift must arise not from the tail and the aft part of fuselage but from the forward part of wing-fuselage combination. The mechanism of the shift in C_y and C_l is not obvious, and it is out of our present discussion because the forward part of flow field is not measured. In the case of flapped configuration (Fig. 36), we also find the shift of C_y and C_l. Moreover, we also find the similar nonlinearities already discussed in the paragraph (2), especially in the variation of C_y. Furthermore, the considerable shift of C_n in the same direction with Fig. 34 is found. The shift of C_n seems to have the possibility of its origin in the similar mechanism of paragraph (2). However, the more data should be required for further discussions. Although the direction of shift is the same as Fig. 34, but the order of shift is sometimes smaller than that of complete model. Then we can suppose that sometimes the vertical tail may have certain contributions on the shift.

Now we should have our attention to the

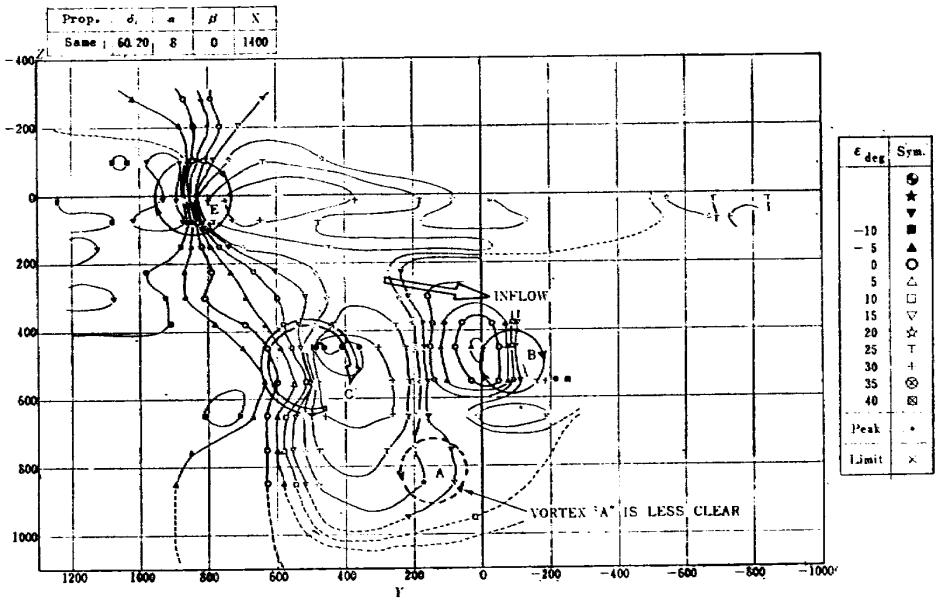

Fig. 37(a) Flow pattern in the case of same rotational direction (down wash field); α=8 degrees, β=0, X=1400 mm

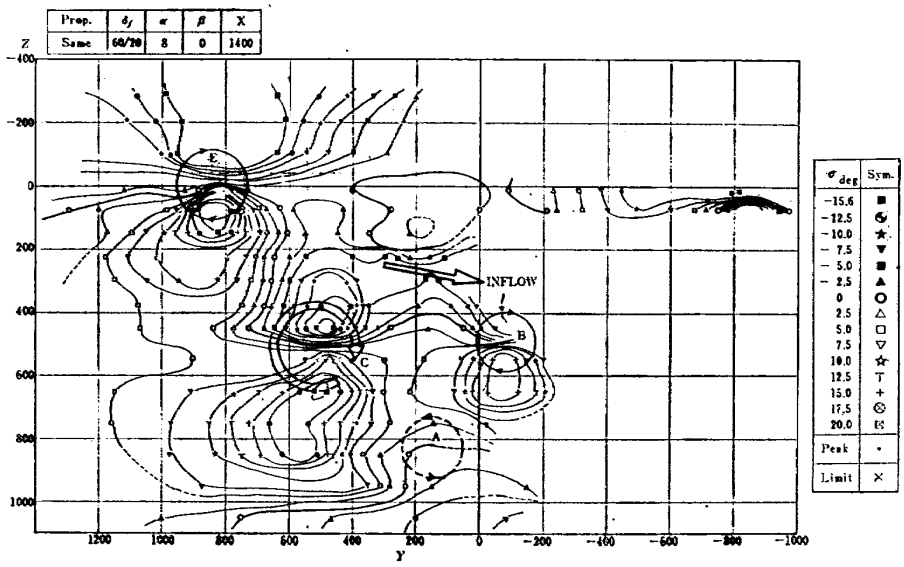

Fig. 37(b) (Continued) (side wash field); α=8 degrees, β=0, X=1400mm

contour maps. The special feature of the flow field is suggested by the inspection of contour maps. As it is seen in Fig. 29(c), the vortical flow pattern develops extensively at the station of midspan of the left wing. This vortical flow corresponds to the vortex shedding from the outer edge of the inner flap. Moreover, from the upper part of this flow, the apparent inflow arises towards the left side of fuselage or towards the bottom of fuselage (see also Fig. 11(a) for the comparison). It is supposed that the rotating flow may play an important role in this development of vortical flow. Thus, obviously the rotation of propeller must have marked influences on the whole flow field. Unfortunately, we have no contour maps around the vertical tail. But it is supposed from the above discussion that the flow field around the vertical tail may be asymmetrical, and may cause a certain shift of yawing moment. Figs. 37 and 38 correspond to the flow pattern sketched in Fig. 29(c). On the other hand, it should be also noticed that the measured shift of C_n in Fig. 34 show us the wide range variation. In the previous measurements the repeated experiments gave us the scattered data on the shift of C_n, even in the same series of measurements. The fact suggests us that the flow field around the vertical tail and aft part of fuselage may be more less stable in this case.

In addition, the drag force of this case is

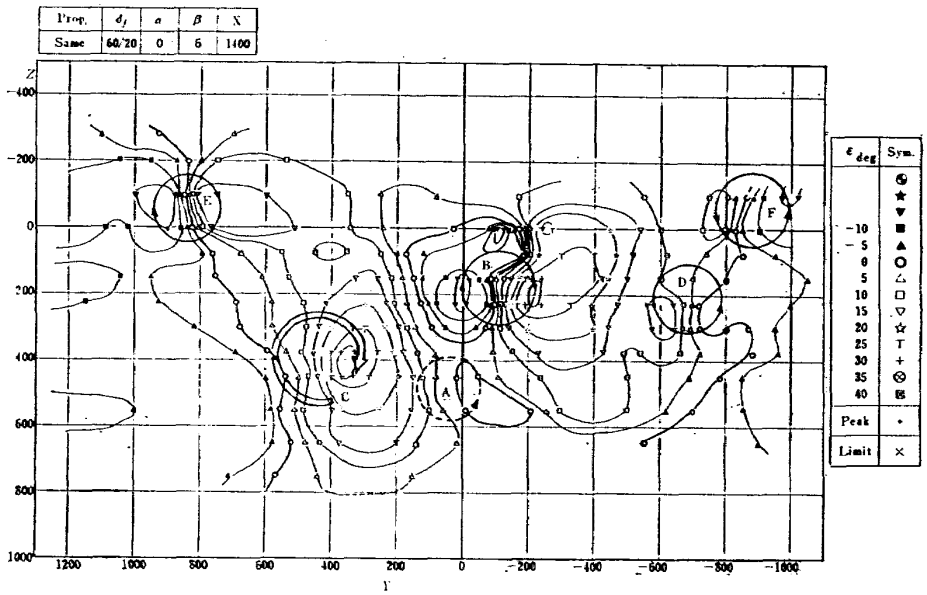

Fig. 38(a) Flow pattern in the case of same rotational direction (down wash field); $\alpha=0$, $\beta=6$ degrees, $X=1400$ mm

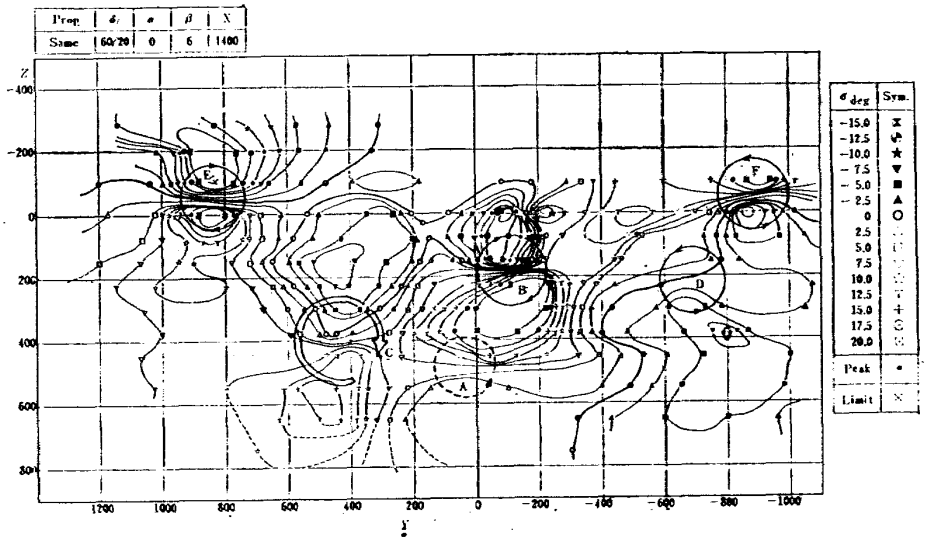

Fig. 38(b) (Continued) (side wash field); $\alpha=0$, $\beta=6$ degrees, $X=1400$ mm

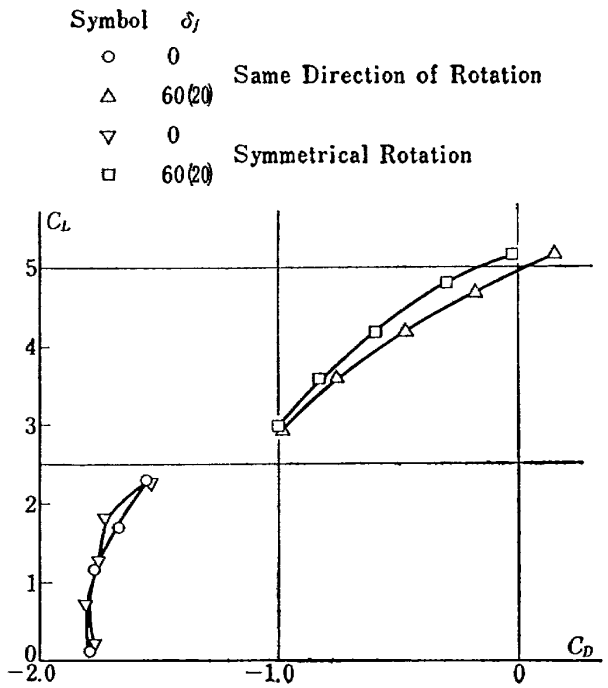

Fig. 39. Lift-drag polar in the force test

greater compared with the case of symmetrical rotation, with the same lift force. The fact is shown in Fig. 39. It is supposed that the increment of drag force may arise only on the left wing, because the flow field must be changed mainly on the left side. The supposition is supported by the comparison of contour maps between Fig. 40 and Fig. 14(c), and also between Fig. 14(c) and Fig. 13(c). In the figures the similar velocity fields are found corresponding to the right side flow region of Fig. 14(c). Therefore, the increment of the drag force is supposed on the left wing, and it may cause the negative shift of C_n.

Consequently we can suppose that the negative shift of C_n and its nonlinear variation may arise from the circulation around the aft part of fuselage, from the asymmetric flow field around the vertical tail and also from the asymmetric increment of the wing drag force. The break down of the whole effects into each contributions still should be avoided. Because those contributions may be closely related with each other, and moreover the flow field around the model is considered to be less stable in this case. For the more conclusive descripition of the phenomena, the theoretical survey must be needed in the future. Also, the more simplified and detailed experiments must be needed in order to investigate the mechanisms further.

10. CONCLUSIONS

In order to investigate the mechanisms of the nonlinear aerodynamic characteristics of the STOL airplane, we have measured the flow patterns in the wake field of the powered model. Contour maps are obtained in many cases. The inspection and qualitative analyses of the results yielded the following conclusions:

(1) The cylindrical surface of slipstream is deformed extensively by the penetration of the wing, by the rotational flow of itself and also by the vortex systems in the whole flow field.

(2) The rotation of propellers affects the intense influences on the flow field through the

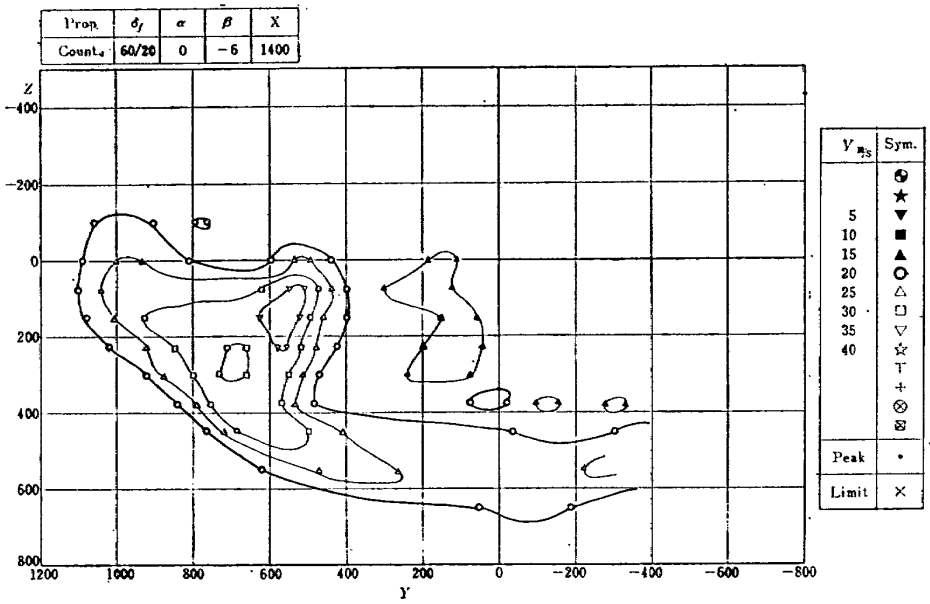

Fig. 40. Velocity contour (cf. Fig. 14(c)), $X=1400$ mm (symmetrical, i.e. counter rotation)

rotating flow in the slipstream. Then, the complicated movements of the vortical flow, namely the movements of the vortex systems are realized in the wake field.

(3) The nonlinear aerodynamic characteristics of the model are confirmed again by the force tests. The mechanisms of these characteristics are verified through the analyses of contour maps. Then, the qualitative understanding of the relations between the characteristics and the wake field are achieved to a certain extent.

(4) The development, the diffusion and the increment of turbulence level of the slipstream are presented. Then, it is considered that the viscous effects have no remarkable influences immediately on the nonlinear characteristics of the model. And in the future the possible predictions will be expected on the nonlinear characteristics through the dynamics of the vortex systems, even in those complicated and nonuniform wake fields.

There are many papers concerning the aerodinamic characteristics of the deflected slipstream STOL airplane. For example, some of them treated the slipstream by the momentum theory,[8] and fair agreement is exhibited with experiments. However, concerning the nonlinear characteristics of the airplane, it is necessary for us to understand the state of affairs in the complicated wake field. There are another many papers showing the results of wind tunnel tests or flight tests on the several types of STOL airplane. However, the survey of flow field related to its characteristics is not found. Then, in this report we have clarified the complexities of this flow field to some extent, with attention to the relations between the aerodynamic characteristics of the model and the structure of the wake field. Of course the wake field of those complicated cases still remains as a "black box" on the whole. We suppose that in the future it is necessary to investigate the dynamics of vortex systems in the nonuniform flow field with the presence of fuselage or any other objects.

ACKNOWLEDGMENTS

For the completion of our measurements, we owe to Dr. Y. Kobashi, Professor of Hokkaido University, who had presented an idea and had developed the new type of velocitymeter in collaboration with Mr. N. Kawahata (one of the authors). The authors wish to express their sincere appreciation to Professor Kobashi for his helpful support. The authors are also grateful to Mr. H. Takagi, Chief of Flight Research Division and to Dr. S. Takeda, Chief of V/STOL Division for their valuable discussion on this work. The authors are also obliged to Mr. H. Araki, Chief of First Airframe Division for his encouragement on this work.

REFERENCES

1) N. Inumaru, and others; Wind tunnel investigations of the twin-propeller deflected slipstream STOL airplane model (I), NAL TM-88, 1966.
2) N. Inumaru, and others; Wind tunnel investigations of the twin-propeller deflected slipstream STOL airplane model (II), NAL TM-107, 1967.
3) N. Kawahata, T. Nakaya; Automatic tracking type flow direction and velocity meter, NAL TM 172, 1970.
4) H.S. Ribner, N. D. Ellis; Theory and computer study of a slipstream, AIAA Paper No. 66–466, 1966.
5) Von J. Stuper; Einflüß des Schraubenstrahls auf Flügel and Leitwerk, Luftfahrtforschung, Vol. 15, No. 4, 1938.
6) H. H. Sweberg; The effect of propeller operation on the air flow in the region of the tail plane for a twin-engine tractor monoplane, NACA WR L-381, 1942.
7) N. Inumaru; The interference of the wing on the discontinuous surface, to be published from NAL.
8) R. E. Kuhn; Semiempirical procedure for estimating lift and drag characteristics of propeller-wing-flap configurations for vertical and short-take-off-and-landing airplanes, NASA MEMO 1-16-59L, 1959.

APPENDIX

List of measurment and contour maps

No. of test	δ_f	Prop.	α	β	X mm	No. of Fig.		
						V	ε	σ
A 1-1	0	Symmetry	0	0	414	17		
A 1-2	0	Symmetry	0	0	918	7	10(a)	10(b)
A 1-3	0	Symmetry	0	0	1405	17		
A 2-1	0	Symmetry	8	0	414			
A 2-2	0	Symmetry	8	0	918	8		
A 2-3	0	Spmmetry	8	0	1405			
A 3-3	0	Symmetry	0	6	1405			
A 3-3	0	Symmetry	0	−6	1405			
A 4-3	0	Symmetry	8	6	1405			
A 4-3	0	Symmetry	8	−6	1405			
B 2-3	0	Same Direc	8	0	1405	9	16(a)	16(b)
C 1-3	60/20	None	0	0	1400			
C 2-3	60/20	None	8	0	1400		20(a)	20(b)
D 1-1	60/20	Symmetry	0	0	414	13(a)	12(a)	12(a)
D 1-2	60/20	Symmetry	0	0	930	13(b)	23(a)	
D 1-3	60/20	Symmetry	0	0	1398	13(c)	23(c)	28
D 2-1	60/20	Symmetry	8	0	415			
D 2-2	60/20	Symmetry	8	0	930		23(b)	
D 2-3	60/20	Symmetry	8	0	1400		23(d)	
D 3-1	60/20	Symmetry	0	6	415			
D 3-2	60/20	Symmetry	0	6	930	30(a)	30(b)	30(c)
D 3-3	60/20	Symmetry	0	6	1400		31(a)	31(b)
D 3′-2	60/20	Symmetry	0	−6	930			
D 3′-3	60/20	Symmetry	0	−6	1400	40	32(a)	32(b)
D 4-1	60/20	Symmetry	8		415			
D 4-2	60/20	Symmetry	8	6	930			
D 4-3	60/20	Symmetry	8	6	1400		33(a)	33(b)
D 4′-2	60/20	Symmetry	8	−6	930	21(a)	21(b)	21(c)
D 4′-3	60/20	Symmetry	8	−6	1400			
E 2-3	60/20	Same Direc.	8	0	1400	15	37(a)	37(b)
E 3-1	60/20	Same Direc.	0	6	415	14(a)		
E 3-2	60/20	Same Direc.	0	6	930	14(b)		
E 3-3	60/20	Same Direc.	0	6	1400	14(c)	38(a)	38(b)

TR-189 The Hybrid Simulation of Guided and Controlled Flight of Rocket	Hajime KOSHIICHI, Masao NAKA, Hidehiko MORI, Noboru OISHI, Akio KANMURI & Kōzō HONMA	Jan. 1970
TR-190 Interaction of Blunt Bodies in Supessonic Flow	Takashi TANI, Iwao KAWAMOTO, Seizo SAKAKIBARA, Junichi NODA & Jiro KONDO	Feb. 1970
TR-191 Drag Measurement in Nearly-Free-Molecule-Flow Regime	Akira ONJI, Kiyoshi YAMAMOTO	Feb. 1970
TR-192T Transient Couette Flow of Rarefied Binary Gas Mixtures	Katsuhisa KOURA	Mar. 1970
TR-193 Simulation Study of Hydraulic Servo System with Consideration of Non-linear Flom Characteristic of Servo Valve	Hajime KOSHIICHI, Takahiro SUZUKI & Mitsuyoshi NAKAMURA	Mar. 1970
TR-194 Guidance Errons —The Effects of the Navigation and Control Systems on the Guided Trajectories—	Koichi MATSUSHIMA, Keiji NIITA, Koji OTSUBO & Toru SHIHO	May 1970
TR-195 Results of Strain and Deflection Measurements Carried out on Model Wings and their Compavison with Calcuteted Resuts	Kazuo KUNO	May 1970
TR-196 Dynamic Stablity Test in Transonic Wind Tunnel Rotary System	Yasujiro KOBASHI, Nagamasa KŌNO, Takenori NISI & Masahumi MIYAZAWA	May 1970

TECHNICAL REPORT OF NATIONAL AEROSPACE LABORATORY
TR-197T

航空宇宙技術研究所報告 197 号 (欧文)

昭和 45 年 5 月 発行

発行所 航空宇宙技術研究所
東京都調布市深大寺町 1,880
電話武蔵野三鷹(0422)44-9171(代表)

印刷所 株式会社 東京プレス
東京都板橋区桜川 2 丁目 27 の 12

Published by
NATIONAL AEROSPACE LABORATORY
1,880 Jindaiji, Chōfu, Tokyo
JAPAN

Printed in Japan